Generalized predictive framework for lateral break-out resistance of submarine pipelines considering nonlinear seabed geometry and consolidation

Corrected proof submitted to *Applied Ocean Research* on 31st October 2021

Bithin GHORAI
Doctoral Candidate
Department of Civil Engineering
Indian Institute of Technology Bombay
Powai, Mumbai – 400 076
India
Email: bithin@iitb.ac.in

Santiram CHATTERJEE
Associate Professor
Department of Civil Engineering
Indian Institute of Technology Bombay
Powai, Mumbai – 400 076
India
Telephone: +91 – 22 – 2576 5327
Fax: +91-22-2576 7302
Email: sc@civil.iitb.ac.in

Susan GOURVENEC
Professor
School of Engineering
University of Southampton
Boldrewood Innovation Campus, Burgess Road
Southampton, SO16 7QF
United Kingdom
Telephone: +44 – 23 – 8059 9139
Email: Susan.Gourvenec@southampton.ac.uk

No. of words: 7056 (without abstract and references)
No. of tables: 8
No. of figures: 16

Generalized predictive framework for lateral break-out resistance of submarine pipelines considering nonlinear seabed geometry and consolidation

Bithin Ghorai [a], Santiram Chatterjee [a,*], Susan Gourvenec [b]

[a] *Department of Civil Engineering, Indian Institute of Technology Bombay, Mumbai – 400 076, India*.
[b] *School of Engineering, University of Southampton, Southampton – SO16 7QF, United Kingdom*.
[*] Corresponding author.

Abstract

The ultimate capacity of submarine pipelines under combined vertical and horizontal loading, so-called lateral break-out resistance, is influenced by the change in seabed geometry due to the installation process and subsequent drainage with associated gain in soil shear strength due to consolidation. The majority of existing solutions in the literature and the current design practices for the assessment of lateral break-out resistance are based on small-strain geometry assumptions and the unconsolidated undrained soil response, i.e. without considering the change in seabed geometry due to installation or improvement in shear strength of the surrounding soil due to post-installation consolidation. In this paper, the effects of installation and subsequent consolidation on the combined load carrying capacity of on-bottom pipelines in a soft clay seabed are investigated and quantified in a systematic manner. A large deformation finite element approach coupled with the Modified Cam Clay plasticity model is adopted to simulate the installation of pipelines, and a series of coupled small strain finite element analyses are performed to study the consolidation and break-out response. A comprehensive range of normalised pipe installation depth, preload level and consolidation time period is considered. Results are interpreted using a critical state framework, and expressed in terms of generalized equations for ease of application in engineering design. A predictive methodology is developed for the estimation of combined load bearing capacity of submarine pipelines in soft clay, including the influences of installation, drainage and consolidated strength.

Keywords: Pipelines; installation; consolidation; bearing capacity; large deformation; design methods.

1. Introduction

Deep-water pipelines are generally installed on the soft seabed sediment without any secondary stabilization measures such as trenching. These pipelines, when remotely installed from a laying vessel in deep-water, embed into the soft soil due to the pipe self-weight and vessel-induced oscillations in the touch-down zone. This results in the formation of soil heave and generation of excess pore-water pressure during installation. During operation, the pipelines convey pressurised high temperature multi-phase flow between the manifold structures and processing platforms, and from there to onshore terminals. The tendency of the pipelines to elongate due to thermal stresses is resisted by friction from surrounding soils, which results in high compressive force on the pipe and causes buckling in the lateral direction. Controlled lateral buckling is preferred to no-buckling so that the high compressive stresses are released. However, design of on-bottom pipelines for controlled buckling requires precise estimation of resistance from the soil. Installation induced soil heave and excess pore-water pressure generated have marked influences on the lateral resistance during pipe break-out. The duration between the commencement of pipe operation and installation varies from a few weeks to months (Krost et al., 2011). During this waiting period, the installation induced excess pore-water pressures dissipate through the seabed, depending on the duration and extent of the load sustained during consolidation. The resulting increase in soil shear strength due to the consolidation process significantly influences the penetration and lateral break-out behaviour of pipelines. Estimation of this post-consolidation soil resistance during controlled lateral buckling is crucial for the accurate and safe design of on-bottom pipelines.

The majority of the previous studies, based on plasticity solutions (e.g. Randolph and White, 2008) and small-strain finite element (SSFE) analysis (e.g. Merifield et al., 2008), focused on the immediate break-out resistance of pipelines and without considering the soil

heave during installation. Large deformation finite element (LDFE) simulations (e.g. Wang et al., 2010, Chatterjee et al., 2012a, Chatterjee et al., 2012b, Ghorai and Chatterjee, 2017) and centrifuge model tests (e.g. Dingle et al., 2008, White and Dingle, 2011, Rismanchian et al., 2019), incorporating the effects of change in seabed geometry, show that soil berms developed around the pipe during installation, have a significant influence on break-out behaviour. However, all these findings are established assuming unconsolidated undrained response of soil during break-out. The consolidation response around a shallowly embedded pipe was first assessed by Gourvenec and White (2010) and then by Krost et al. (2011) assuming elastic soil behaviour. Elastoplastic coupled consolidation response of pipelines has since been studied using the Modified Cam Clay (MCC) soil constitutive model within the LDFE framework (e.g. Chatterjee et al., 2012c, 2013); Chatterjee et al. (2012c) only considered the pipe installation – not the lateral break-out; Chatterjee et al. (2013) studied the lateral break-out response including installation, but only for a single pipe weight (corresponding to full bearing capacity) and consolidation time (corresponding to ~100% pore pressure dissipation). Later, Chatterjee et al. (2014) considered a range of pipe weights and degrees of consolidation to study break-out response using a critical state framework, but the installation process was not modelled, and the pipe is assumed to be 'wished-in-place' (WIP) at a particular embedment. In the WIP condition, a pipe is pre-embedded at a particular depth, with the consideration of flat seabed adjacent to the pipe. In reality, the seabed geometry continuously changes during the process of installation and a WIP pipe does not replicate this scenario. Previous research efforts (e.g. Wang et al., 2010, Chatterjee et al., 2012a, Chatterjee et al., 2012b, Ghorai and Chatterjee, 2017) highlighted the potential of the LDFE approach to simulate pipe installation process, by advancing the pipe into the soil in small incremental depths to reach a target embedment. It was shown that the pipe break-out resistance is under-predicted using the WIP approach as it does not account for the soil berms developed adjacent to the pipe during installation and it is

thus important to consider the effects of installation on pipe break-out response. Cocjin et al. (2018) present results from centrifuge modelling investigating the effects of softening and consolidation on axial and lateral response of pipelines in soft clay following monotonic and cyclic installation. The observed lateral break-out resistance was interpreted within the critical state framework but by the nature of physical model testing, a comprehensive range of variables (e.g., pipe embedment and degree of consolidation) could not be addressed.

The limitations of the previous studies are systematically addressed in this research using a MCC soil model in LDFE framework (Chatterjee et al., 2012c). At first, the pipe is installed to various target embedment levels over a short period of time, simulating unconsolidated undrained soil behaviour. It is to be noted that dynamic effects during pipe laying may influence the penetration response. Westgate et al. (2009) reported that the pipeline embedment is increased (in addition to the embedment due to self-weight penetration) due to vessel-induced oscillations during laying, caused mainly by the ocean waves (wave height and direction). It is also highlighted in the study that the influence of current loading on pipe installation response is not significant. The additional pipe embedment due to the laying process is considered indirectly in the present analysis by modelling over-penetration. The pipe was unloaded to different fractions of vertical unconsolidated undrained capacity at a particular embedment, equivalent to various pipe operative loads during consolidation. Various waiting periods (degrees of consolidation) are also considered in the consolidation stage. Subsequently, the undrained break-out is carried out in all possible pipe directions to derive failure envelopes in vertical-horizontal (V-H) load space. The novelty in this study is to explore a comprehensive range of variables and encapsulate the findings into a generalized predictive model for a range of pipe weights, embedment depths, and degrees of consolidation, including nonlinear seabed geometry and consolidation to enable prediction of break-out response of on-bottom pipelines.

2. Numerical Methodology

2.1 LDFE analysis with RITSS approach

Large deformation finite element (LDFE) analysis based on 'remeshing and interpolation technique with small strain' or RITSS (Hu and Randolph 1998a, Hu and Randolph 1998b) was carried out to simulate the pipe installation process. The MCC constitutive model based on critical state soil mechanics (Roscoe and Burlund, 1968) and implemented in RITSS by Chatterjee et al. (2012c), was used to capture changes in undrained strength as a result of pipe installation and consolidation. To simulate pipe installation down to a target embedment, the whole depth was discretized into numbers of small depth increments (incremental pipe displacements) and in each increment, Lagrangian analysis was performed in the commercial finite element (FE) software Abaqus (Dassault Systèmes, 2013). The soil geometry was then redrawn incorporating the shape of the deformed boundary and a new mesh was generated. The effective stresses, void ratios, pore-water pressures, and the current sizes of yield envelope (determined by pre-consolidation pressure p'_c) – were then all mapped from the old mesh to a new mesh. With these mapped variables as initial conditions, the next incremental analysis was conducted in Abaqus. The remeshing of domain and mapping of variables was continued until the pipe reached target embedment. All these operations were automatically executed by a Fortran program that interacts continually with several Fortran subroutines (for mapping of variables) and Python scripts (for FE model generation, small strain analysis and accessing results) to perform the LDFE analysis. The details of the RITSS technique combined with a MCC plasticity soil model can be found in previously published papers (e.g. Chatterjee et al., 2012c, Chatterjee et al., 2013).

2.2 Details of finite element model

Two-dimensional (2D) plane strain conditions are considered for the installation, consolidation and subsequent break-out analysis of pipelines. A pipe of diameter D was installed to various depths (w) in a soft clay seabed. The lateral soil boundaries were positioned

at a distance of 8*D* on either side of the pipe centre and the base boundary was set at 10*D* below the pipe invert. These distances were carefully chosen to avoid any boundary effects. Roller and pinned supports were provided for the lateral and base boundaries, respectively. The seabed surface was permitted to act as a drainage boundary through which pore-water pressures could dissipate. However, it should be noted that the surface of the pipe remaining in contact with the soil was considered impermeable. Also, drainage was not allowed through the lateral and base boundaries. A schematic representation of the problem geometry is shown in Fig. 1.

In the FE model, the pipe was considered as a rigid body and the soil as a deformable half space. The interface between the pipe and the soil was taken as perfectly smooth with zero shear stresses mobilized at the interface. Note that the interface roughness between pipe and soil would affect the response and a rough interface would be expected to generate more excess pore-water pressure and therefore provide greater strength increase and higher break-out resistance than a smoother interface. Hence, the smooth pipe-soil interaction considered in this study, provides the lower estimate of actual break-out resistance. A hard contact with separation allowed was prescribed in the normal direction. The soil domain was discretized with six-noded modified displacement and pore pressure plane strain elements, with hourglass control (CPE6MP) available in the Abaqus/Standard element library. A typical FE mesh prior to the installation of the pipe is superimposed on the problem geometry in Fig. 1. The mesh was optimized to balance accuracy with computational time needed for analyses. In order to achieve this, a near field zone surrounding the pipe with a horizontal extent of 3*D* and a vertical extent of 1*D* was created with minimum size of element = 0.03*D*.

The soil was considered to be weightless in the present study and the influence of soil weight directly superposed with the shearing resistance to evaluate the bearing capacity factors, as commonly adopted (e.g.Chatterjee et al., 2012a, 2014, Merifield et al., 2009, Martin and White, 2012). An artificial uniform surcharge (σ'_{v0}) of 10 kPa is placed on the free surface of

the weightless soil, that results in uniform distribution of strength with depth, due to the constant ratio between undrained strength and effective overburden stress. The advantage of modelling this strength uniformity is that the initial coefficient of consolidation (c_v) also becomes invariant with depth. This makes normalization of consolidation periods (T) simpler due to the constant value of c_v. The present study considers a uniform strength seabed to enable comparison with published WIP small-strain solutions (Chatterjee et al., 2014) modelling the same strength profile. A linearly increasing strength profile for normally consolidated/lightly over-consolidated clays would affect the vertical penetration response and would be expected to mobilize more soil resistance (e.g. Chatterjee et al., 2012a, Ghorai and Chatterjee, 2017, Chatterjee at al., 2012c, Martin and White, 2012, Dutta et al., 2015). However, for soft seabeds (e.g. $s_u = 2 + 1z$ kPa) and pipe diameters of < 1 m, the local heterogeneity ratio for the zone of failure mechanism is small (i.e. kD/s_{u0} close to zero, where k = strength gradient, D = pipe diameter and s_{u0} = shear strength at pipe invert level). Therefore, the uniform strength profile considered in this study is likely to give a good indication of the lateral break-out resistance for normally and lightly over-consolidated clays.

2.3 Soil constitutive model

The clay plasticity model available in Abaqus/Standard is based on the classical Modified Cam Clay (MCC) model (Roscoe and Burland, 1968) and has been used to simulate the soil behaviour in the present study. The model parameters chosen for the present numerical analysis are similar to those of kaolin clay used in the experimental studies in the University of Western Australia (Stewart, 1992) and are listed in Table 1. In the MCC soil model, the yield envelope is represented by an ellipse of the form:

$$\left(p'\right)^2 - p'p'_c + \left(\frac{q}{M}\right)^2 = 0 \tag{1}$$

where, p'_c is the pre-consolidation pressure that generally controls the initial size of the envelope. Since the soil was considered to be isotropic (K_0 = 1) and weightless in this study, the size of the initial envelope is determined by the initial mean effective stress p'_0 (p'_c being equal to p'_0). The constant M represents the slope of critical state line (CSL) in mean effective - deviatoric (p'-q) stress space. The value of M (= q/p') depends on the critical state soil friction angle (φ'_{cs}) and can be experimentally obtained from laboratory triaxial tests. In the MCC plasticity model, the elastic soil response inside the yield surface is defined by a porous elastic material and the elastoplastic soil response is represented by a standard elliptical yield function (yield surface size parameter β_{yield} = 1 is specified on the 'wet' side of CSL for symmetric ellipse) as described in Eq. (1). It is to be noted that associative flow rule is prescribed in the analysis. Furthermore, a hardening parameter in terms of the initial size of yield envelope (a_0 = $p'_c/2$) is defined in the clay plasticity model. The evolution of this parameter (a_0) accounts for the expansion (strain hardening) of the yield surface during installation to various depths in normally consolidated deposits.

The initial void ratio (e_0) in the soil at any depth can be obtained from the critical state theory as follows:

$$e_0 = e_{cs} - (\lambda - \kappa)\ln\left(\frac{p'_c}{2}\right) - \kappa \ln\left(p'_0\right) \tag{2}$$

where, e_{cs} represents the void ratio on CSL corresponding to 1kPa mean effective stress (p'); λ and κ are the slope of normal consolidation line (NCL) and unloading-reloading line (URL), respectively. The undrained shear strength ratio of soil R is the normally consolidated strength ratio between undrained shear strength (s_u) and effective vertical stress (σ'_v). This ratio is not an input parameter in MCC analysis, and can be derived using the critical state concepts for plane strain conditions (Wroth,1984):

$$R = \frac{s_u}{\sigma'_v} = \frac{2}{\sqrt{3}}\left(\frac{\sin\phi'_{cs}}{2a}\right)\left(\frac{a^2+1}{2}\right)^{\left(\frac{\lambda-\kappa}{\lambda}\right)} \tag{3}$$

where, the parameter a is defined as:

$$a = \frac{3-\sin\varphi'_{cs}}{2\left(3-2\sin\phi'_{cs}\right)} \tag{4}$$

The initial undrained shear strength, $s_{u,ini}$ using Eq. (3) (see Table 1 for MCC parameters) is found to be 2.86 kPa. Since all the results presented in this research are normalized with respect to the obtained $s_{u,ini}$ value, they become non-dimensional and hence the absolute value of s_u is not important in the study.

2.4 Programme of analyses

Analyses were carried out in three stages: (I) undrained installation, (II) consolidation under specific preload, and (III) consolidated undrained (CU) break-out. Unconsolidated undrained (UU) analyses were also performed to quantify the gain in capacities due to consolidation. During stage (I), the pipe was incrementally installed to various depths (w/D = 0.25, 0.5, and 1) in an undrained manner using a coupled LDFE approach. The pore-water pressures were not allowed to dissipate at this stage. An incremental displacement of δ/D = 1% was applied at the pipe centre (defined as reference point) to penetrate the pipe into the soft soil. The incremental displacement is selected in a way to preclude any element distortions in the high stress (or strain) concentration zone under the pipe, as well as to execute the entire LDFE simulation in an accurate and efficient manner. Additional analyses with pipe incremental displacements of 0.5% D and 2% D confirmed that the chosen increment of 1% D is appropriate for the present boundary value problem.

After installation, the pipe was preloaded with a pre-defined fraction of the unconsolidated undrained vertical capacity ($V_{max,UU}$) at that depth and a coupled consolidation analysis was performed under the preload (V_p = 0.3 $V_{max,UU}$, 0.6 $V_{max,UU}$, 0.75 $V_{max,UU}$, and 0.9 $V_{max,UU}$) to simulate drained conditions during stage (II). The installation induced excess pore-water pressures were permitted to dissipate through the drainage boundary (explained in section 2.2 and Fig. 1) and the vertical displacement of the pipe was freed to allow settlement under the particular preload during the process of consolidation.

The effects of installation and consolidation on the undrained break-out response were studied in stage (III) using coupled small-strain finite element (SSFE) analysis. In this stage, displacement probe tests were conducted in various directions, encompassing a range of possible pipe trajectories (θ = 0° to 180° in increments of 30°) to derive failure envelopes in *V*-*H* load space. Drainage through the seabed was not permitted during break-out, and a combination of pipe displacements (as a function of the probe angle) was applied at the reference point to mobilize the peak horizontal resistance in each direction - defined as the pipe break-out capacity corresponding to that probe angle. The different cases of preload level, consolidation time and pipe break-out directions considered during these stages are summarized in Table 2.

2.5 Benchmarking of results

The results from the present coupled LDFE analysis are benchmarked against the upper-bound plasticity solution by Randolph and White (2008). It is a common exercise to validate results of effective stress LDFE analysis (modelling unconsolidated undrained soil response) with the total stress solutions based on Tresca yield criterion (e.g. Chatterjee et al., 2012c, Chatterjee et al., 2013, Ansari et al., 2014, Mahmoodzadeh et al., 2014, Mahmoodzadeh et al., 2015, Schneider et al., 2019). At first, the pipe is installed to a depth of w = 0.5D in

weightless uniform soil. The pipe-soil interface is considered as smooth, with separation being allowed at the interface. As the pipe penetrates into the soil, excess pore-water pressures are developed around the pipe because of high penetration rate and low permeability ($vD/c_v > 100$). The penetration resistance after each incremental analysis is measured and normalized with Ds_u to obtain the vertical bearing capacity factor (V/Ds_u). The variation of normalized resistance with penetration depth is shown in Fig. 2. An additional LDFE analysis was also performed within the total stress framework based on Tresca yield criterion, by adopting an equivalent s_u value estimated from Eq. (3). Also presented are the results of a plasticity-based model, developed from the analysis of centrifuge experiment observations (Hodder and Cassidy, 2010), and pushed-in-place (PIP) FE analysis (Merifield et al., 2009) (see Fig. 2). It is observed that the penetration resistances in Tresca LDFE and PIP-FE analyses are in good agreement with the theoretical plasticity solution at the final penetration depth. This is due to the assumption of weightless soil in the present LDFE analysis for which the penetration resistance is unaffected by the formation of soil berms during installation. For the coupled LDFE analysis, the installation resistance obtained is greater (~7.4%) than the corresponding Tresca case because of the differences in the yield surfaces on the deviatoric plane (hexagonal surface in Tresca vs circular surface in MCC), considered in the respective constitutive models. This is consistent with the previous studies of large deformation penetration problems for piezo probes (e.g. Mahmoodzadeh et al., 2015, Schneider et al., 2019). The results of LDFE analysis with MCC model matches reasonably well with the centrifuge test result.

After installation, unconsolidated undrained (UU) break-out analyses were performed to compare the pipe response with classical plasticity solutions (Randolph and White, 2008). Displacement-controlled probe tests were conducted to obtain the points on the failure envelope at $w/D = 0.5$. The vertical (V) and horizontal (H) resistances mobilized during break-out, normalized with Ds_u are presented in Fig. 3. Failure envelopes of an upper-bound solution

and equivalent Tresca-LDFE analysis are also compared in the same figure. It is observed that the size of the envelope increases in the Tresca-LDFE case compared to the upper bound solution at lower vertical load levels. This is because of the soil berms formed around the pipe during installation. At lower vertical load, the pipe tends to move upward, and the effect of berms is more significant, resulting in greater soil zone of shearing. PIP solutions (Merifield et al., 2009) for pure vertical and horizontal pipe movements, and an envelope predicted by Hodder and Cassidy (2010) are also compared in the same figure. The difference between the sizes in failure envelope obtained from centrifuge tests (Hodder and Cassidy, 2010) and Tresca LDFE analysis is evident in Fig. 3. Also note that at zero vertical load, no horizontal resistance ($H/Ds_u = 0$) is developed in the present study, whereas soil resistance ($H/Ds_u \sim 1.6$) is mobilized at $V = 0$ in the centrifuge study. This is due to suction developed within the soil mass at the rear end of the pipe during break-out that does not allow immediate separation of the pipe in the physical model test. This phenomenon has not been modelled in the present study and immediate pipe breakaway is considered. The envelope obtained from MCC analysis shows an approximate 9.3% increase in peak horizontal resistance compared to the corresponding Tresca case.

The validation analyses have demonstrated that the LDFE model used for this study captures the undrained response under vertical penetration and lateral break-out defined by theoretical upper-bound analysis.

3. Results and Discussions

In this section, results from a comprehensive parametric study are presented to assess the consolidated undrained break-out response of pipelines.

3.1 Undrained installation response

The variation of installation resistance normalized by Ds_u with penetration depth, from the LDFE analysis is shown in Fig. 4 for $w/D = 1$. The estimated bearing capacity factor at the target installation depth is $V/Ds_u \approx 5.6$. The normalized installation resistance from a centrifuge test (Cocjin et al., 2018) in soft clay deposit is also compared in the same figure. The resistance contribution from soil self-weight ($f_{bv}A_s\gamma'$, where f_{bv} is the buoyancy factor for vertical penetration, taken as 1.0; A_s is the submerged pipe area in soil; and γ' is the buoyant unit weight of soil) is deducted to compare with the bearing capacity factor in weightless soil. The difference in installation resistances between present study and centrifuge experiment is attributed to the different pipe-soil interface (rough) and strength profile ($s_u = 0.1 + 0.7z$ kPa) considered in the physical model test.

Since the pipe is installed within a short period of time, excess pore-water pressures around the pipe cannot dissipate through the heaved seabed due to high penetration rate and low soil permeability ($vD/c_v > 100$). This undrained behaviour of soil leads to development of excess pore-water pressures (Δu) surrounding the pipe. The contours of excess pore-water pressure throughout the soil domain, normalized by the maximum value at the pipe invert, is shown in Fig. 5 for different embedment depths. The contours illustrate that the maximum pore pressure develops just beneath the pipe and gradually decreases with the distance from invert, as would be expected. The excess pore pressure field ranges from a depth of ~1.5D below the pipe at $w/D = 0.25$, increasing to ~3.5D at $w/D = 1$.

3.2 Consolidation under different pipe self-weight

Coupled consolidation analyses were conducted to study the pore pressure dissipation time histories under different pipe weights ($V_p/V_{max,UU}$) after installation. Full primary consolidation of soil is achieved by allowing adequate time for all the installation induced excess pore-water pressures (Δu) to completely dissipate through the seabed surface. The

normalized consolidation time (T) required for the Δu to become negligible is calculated as $T = c_v t/D^2$, where c_v represents the initial coefficient of consolidation that can be expressed as:

$$c_v = \frac{k\left(1+e_0\right)p_0'}{\lambda\gamma_w} \tag{5}$$

Here, k is the permeability of soil, and γ_w is the unit weight of water. All other terms are described in Eq. (2). The normalized excess pore pressure variations near the pipe invert under different preload levels ($V_p/V_{max,UU}$ = 0.3, 0.6, 0.75 and 0.9) at w/D = 0.25 are shown in Fig. 6(a). The excess pore pressures (Δu) are normalized with respect to the initial value ($\Delta u_{i,\,p}$) after being unloaded to V_p from $V_{max,UU}$ at that depth. It is observed that the trend in excess pore pressure variation remains constant until T~0.01, and then gradually decreases to zero at T~2. The decay in excess pore pressure with time can be suitably described by a sigmoid function:

$$\frac{\Delta u}{\Delta u_{i,\,p}} = \frac{1}{1+\left(T/T_{50}\right)^m} \tag{6}$$

where, T_{50} represents the normalized consolidation time to dissipate 50% of excess pore-water pressure near the pipe invert and m is a fitting parameter. Dissipation time histories are also obtained for other embedment levels (w/D = 0.5 and 1) and the fitted expressions of ($\Delta u_i/\Delta u_{i,p}$) [Eq. (6)] for these depths are presented in Fig. 6(b). Curve fitting parameters T_{50} and m for all installation depths are summarized in Table 3. Also presented are the results from a centrifuge model test (Cocjin et al., 2018) at w/D = 0.5 for a rough pipe, that shows reasonable agreement with the present LDFE analysis. The dissipation responses of a corresponding WIP pipe (Chatterjee et al., 2014) are plotted in the same figure to understand the behaviour of soil without the installation effect. It is observed that the rate of excess pore pressure dissipation is slower in the LDFE analysis compared to the SSFE analysis (T_{50} value is 1.5 times higher in the LDFE analysis compared to the SSFE analysis at w/D = 0.5 in Fig. 6(b)). The delayed

response in the LDFE analysis is due to the presence of soil berms on either side of the pipe causing a longer drainage path. The shape of the dissipation curves in the LDFE analyses during the initial phase of consolidation is also different from the SSFE results, demonstrating the differences in the amount of excess pore pressure dissipated through the seabed, with more pronounced effect at shallow depths (compare $\Delta u_i / \Delta u_{i,p}$ for $w/D = 0.25$ in LDFE against $w/D = 0.2$ in SSFE at $T = 0.001$). Therefore, it is necessary to model the installation process (through LDFE analysis) to capture the excess pore pressure decay response accurately that governs the rate of effective normal stress development around the pipe and thus the rate of gain in soil shear strength.

The initial installation depth (w/D) of the pipe increases due to the dissipation of excess pore-water pressure during consolidation under various pipe weights. The consolidation settlement variations ($\Delta w_c/D$) as a function of non-dimensional time (T) are shown in Fig. 7 at $w/D = 0.25$. As expected, the final settlement of pipe increases with the increase in $V_p/V_{max,UU}$. The pipe heaves slightly (in an upward direction) at the beginning of consolidation when preloaded to a relatively lower value ($V_p/V_{max,UU} = 0.3$). However, with the increase in preload, the heave of the pipe becomes minimal, and it gradually settles down into the soil as the excess pore-water pressure dissipates.

3.3 Consolidated and unconsolidated undrained break-out response

The break-out response during lateral movement of a pipe depends on the shear strength of surrounding soil after post-installation consolidation. Failure envelopes in V-H load space are derived to represent the combination of loads at which pipe break-out occurs. Due to the normality condition, the trajectory of the pipe can also be determined by drawing a normal to these envelopes. The fully consolidated undrained (CU) envelopes at different embedment levels ($w/D = 0.25$, 0.5 and 1) under various preloads are presented in Fig. 8. Results from the

unconsolidated undrained (UU) case are also shown in the same figure. The vertical and horizontal resistance responses in the failure envelopes are normalized with the unconsolidated undrained shear strength (s_u) at pipe invert level and the diameter (D) of pipe. Equivalent predictions from SSFE analysis (Chatterjee et al., 2014) are also presented in Fig. 8(b) for the case $w/D = 0.5$. The envelopes in LDFE analysis are slightly asymmetric in shape, and the sizes are slightly greater at lower vertical loads compared to the SSFE envelopes. The peak horizontal resistance obtained in LDFE analyses is 10-12% higher (with increasing $V_p/V_{max,UU}$) than the corresponding SSFE predictions (compare the CU envelopes in LDFE and SSFE analyses for $V_p/V_{max,UU} = 0.75$ and 0.9). Maximum break-out resistance at $w/D = 0.5$ from the centrifuge experiment (Cocjin et al., 2018) under $V_p/V_{max,UU} = 1.0$ is also plotted in Fig. 8(b). Note that these normalized resistances are obtained after buoyancy corrections (assuming vertical and horizontal buoyancy factors, f_{bv} and f_{bh} as unity) to compare with the weightless soil case in the present study. The effect of consolidation is more apparent at shallow embedments, resulting in an increase in peak break-out resistance of up to 50% at $w/D = 0.25$ (see Fig. 8(a)). This is because of the passive resistance from the soil berm adjacent to the pipe during break-out. The WIP solution does not capture this effect and therefore underpredicts the break-out capacity.

The greater size of CU envelopes compared to the corresponding UU envelope at any embedment depth is clear from the Fig. 8. The increases in maximum break-out resistance are 62.5%, 54% and 45% at $w/D = 0.25$, 0.5 and 1, respectively for the preload, $V_p/V_{max,UU} = 0.9$. The gain in CU capacities from the UU capacity is due to the dissipation of excess pore-water pressures around the pipe that results in an enhancement of soil shear strength. For the CU cases, the envelopes increase in size with increasing preload as expected. A maximum variation of ~33% in consolidated vertical bearing capacity is observed due to the change in $V_p/V_{max,UU}$ from 0.3 to 0.9. Interestingly, the variation is decreased from ~33% to ~27% with the increase

in w/D from 0.25 to 1, demonstrating the significance of consolidation at shallow embedments. The increase in shear strength due to full primary consolidation under different preloads can be visualized from the contour diagrams as illustrated in Fig. 9 for w/D = 0.25. The maximum ratio of consolidated shear strength to initial strength ($s_{u,cons}/s_{u,ini}$) around the pipe is ~2 for $V_p/V_{max,UU}$ = 0.9 and it becomes ~1.3 as the preload is decreased to 0.3. The consolidated shear strength ($s_{u,cons}$) is dependent on the change in void ratio between initial (e_0) and final states (e_{cons}) during consolidation, and can be evaluated as:

$$s_{u,cons} = s_{u,ini} \exp\left(\frac{e_0 - e_{cons}}{\lambda}\right) \tag{7}$$

The zone of enhanced strength under the pipe also increases in size with the increase in pipe weight. The depth wise expansion is approximately 0.5D to 2D below the pipe invert as the preload increases from 0.3 to 0.9. This enhancement in soil strength surrounding the pipe due to consolidation essentially governs the gain in ultimate capacities and associated pipe movements during lateral break-out.

The partially consolidated, undrained (PCU) break-out responses of the pipe were further investigated under various preloads at different embedment levels. The V-H envelopes at various installation depths for non-dimensional consolidation times T = 0.05 and 0.5 (corresponds to approximately 30% and 75% excess pore-water pressure dissipation) (see Table 2) are presented in Figs. 10 and 11, respectively. The figures illustrate that the size of the envelopes increase from the UU case due to partial dissipation of excess pore-water pressure adjacent to the pipe. The maximum increases in break-out resistance for T = 0.05 are 20.2%, 11.2% and 5.6% at w/D = 0.25, 0.5 and 1, respectively for $V_p/V_{max,UU}$ = 0.9. The gradual build-up in maximum horizontal resistance ($H_{max,PCU}$) due to partial drainage across the seabed surface progresses with time and the degree of partial consolidation depends on the non-dimensional time (T) and the preload value (V_p). For example, the ultimate horizontal capacity

of on-bottom pipelines is improved after an elapsed time of ~ 107 days (considering $T = 0.5$ that corresponds to a degree of consolidation ≈ 75% and initial c_v estimated from Eq. (5)), by 53.6%, 40.1% and 27.4% at $w/D = 0.25$, 0.5 and 1, respectively under the preload $V_p/V_{max,UU} = 0.9$ (Fig. 11).

4. Development of Generalized Prediction Model

4.1 Maximum unconsolidated undrained capacity

The maximum, unconsolidated, undrained vertical and horizontal resistances ($V_{max,UU}$ and $H_{max,UU}$) are obtained for pure vertical and horizontal pipe movements following the installation to a desired penetration depth. The variation of these resistances with installation depth is shown in Fig. 12, which can be described by simple power equations:

$$\frac{V_{max,UU}}{Ds_u} = a_u \left(\frac{w}{D}\right)^{b_u} \tag{8}$$

$$\frac{H_{max,UU}}{Ds_u} = c_u \left(\frac{w}{D}\right)^{d_u} \tag{9}$$

In the above equations, a_u, b_u, c_u and d_u are the fitting coefficients with the values listed in Table 4. These unconsolidated ultimate capacities are used to normalize the fully or partially consolidated, ultimate resistance responses in the subsequent sections.

4.2 Maximum consolidated undrained capacity

The maximum, fully consolidated, undrained vertical ($V_{max,CU}$) and horizontal ($H_{max,CU}$) capacities are estimated for each of the preload levels and normalized with their respective maximum unconsolidated ($V_{max,UU}$ or $H_{max,UU}$) values. The variations of $V_{max,CU}/V_{max,UU}$ and $H_{max,CU}/H_{max,UU}$ with the preload are shown in Fig. 13 at various pipe embedment depths. These variations can be appropriately described by generalized power expressions:

$$\frac{V_{\max,CU}}{V_{\max,UU}} = 1 + a_d \left(\frac{V_p}{V_{\max,UU}} \right)^{b_d} \tag{10}$$

$$\frac{H_{\max,CU}}{H_{\max,UU}} = 1 + c_d \left(\frac{V_p}{V_{\max,UU}} \right)^{d_d} \tag{11}$$

where, the best-fit coefficients (a_d, b_d) are used for the maximum, fully consolidated vertical capacity and (c_d, d_d) for the maximum, fully consolidated horizontal capacity. Table 5 summarizes the values of these coefficients for different installation depths.

The analytical framework proposed by Gourvenec et al. (2014) for surface foundations to assess the development of consolidated, undrained vertical capacity due to the enhancement of soil shear strength after full primary consolidation has been implemented here, as previously done by Chatterjee et al. (2014) for WIP pipelines. The gain in shear strength (Δs_u) after full primary consolidation under the preload, V_p is expressed as:

$$\Delta s_u = f_\sigma f_{su} R \left(\frac{V_p}{D_{eff}} \right) \tag{12}$$

Here, $f_\sigma f_{su}$ is a combined scaling parameter in normally consolidated soil to account for the non-uniform stress and strength distribution in the influence zone around the pipe undergoing consolidation. It should be noted that the single parameter $f_\sigma f_{su}$ can be decoupled into two separate scaling factors to capture the behaviour in over consolidated deposits (Gourvenec et al., 2014). The parameter R used in Eq. (12) represents the strength ratio as obtained from Eq. (3) and is equal to 0.286 for the soil parameters considered in the study. D_{eff} is the effective diameter of the pipe in contact with the soil and can be determined as:

$$D_{\text{eff}} = D\sin\left\{\cos^{-1}\left(1-\frac{2w}{D}\right)\right\} \text{ for } \frac{w}{D} \le 0.5$$
$$= D \text{ for } \frac{w}{D} > 0.5 \tag{13}$$

The gain in ultimate, consolidated undrained, vertical capacities normalized with their corresponding unconsolidated undrained values due to preloading at different depths is presented in Fig. 14(a). The improvement in maximum consolidated resistance is linked with the enhancement of soil strength due to consolidation (e.g. Chatterjee et al., 2014, Gourvenec et al., 2014, Feng and Gourvenec, 2015, Stanier and White, 2019) as per the following equation:

$$\frac{V_{\text{max,CU}}}{V_{\text{max,UU}}} = 1 + \frac{\Delta s_{\text{u}}}{s_{\text{u,ini}}} = 1 + f_{\sigma} f_{\text{su}} R\left(\frac{V_{\text{p}}}{D_{\text{eff}} s_{\text{u,ini}}}\right) \tag{14}$$

In Eq. (14), the combined parameter $f_{\sigma}f_{\text{su}}$ for normally consolidated deposits is varied to best-fit the LDFE results and the values are tabulated in Table 6. The $f_{\sigma}f_{\text{su}}$ parameter is found to be constant and equal to 0.45 for $w/D \le 0.5$, the same as that derived in WIP analysis (Chatterjee et al., 2014), for pipe embedments up to 0.5D. The similar values of $f_{\sigma}f_{\text{su}}$ obtained in the LDFE and SSFE analysis indicate similar proportional increase in capacity due to consolidation, relative to the unconsolidated undrained capacities - and not similar absolute unconsolidated or consolidated undrained capacities. Fig. 8 clearly shows the additional absolute capacity available by considering the pipe penetration process. For pipe embedments greater than 0.5D, as considered in the present study (e.g. w/D = 1), a lower $f_{\sigma}f_{\text{su}}$ value of 0.32 was obtained. The lower scaling coefficient is to be expected at greater pipe embedments as the failure mechanism for deeper embedments transitions from the that observed at lower embedments where the mechanism reaches the soil surface, to a confined mechanism over a relatively small area under the pipe. The relative increase in pipe capacity is therefore lower at w/D > 0.5 as the failure mechanism does not significantly overlap with the zone of enhanced shear strength. Equivalent

results for surface strip footings with the scaling parameters adopted from Gourvenec et al. (2014) are also presented in the same figure. It is observed that the ultimate capacities estimated using these parameters are relatively less than those obtained for pipelines.

The approach described above is also employed to determine the maximum, consolidated, undrained break-out resistance ($H_{max,CU}$). The variation of $H_{max,CU}/H_{max,UU}$ with the preload V_p at various depths is shown in Fig. 14(b). The coupling effect between the ultimate horizontal capacity development and shear strength enhancement in soil due to consolidation can be described as (e.g. Feng and Gourvenec, 2015, Stanier and White, 2019):

$$\frac{H_{max,CU}}{H_{max,UU}} = 1 + \frac{\Delta s_u}{s_{u,ini}} = 1 + f_\sigma f_{su} R \left(\frac{V_p}{D_{eff} s_{u,ini}} \right) \tag{15}$$

To suitably fit the ultimate consolidated break-out responses [Eq. (15)], different combined scaling parameters ($f_\sigma f_{su}$) at various depths are obtained with the values summarized in Table 6. The gain in ultimate horizontal capacitiy is greater than the gain in ultimate vertical capacity, as evident from the range of combined scaling parameter $f_\sigma f_{su}$ (refer to Table 6). The $f_\sigma f_{su}$ value increases by 67% with the decrease in w/D from 1.0 to 0.25. The higher value at lower embedment is attributed to the large overlap between the soil displacements within the failure mechanism during pipe break-out and the influence zone of consolidated shear strength. At greater depths, the zone of improved strength is mostly confined under the the pipe and the failure at breakaway occurs within the soil berms adjacent to the pipe near the seabed. Thus, the overlap in the mechanism with the consolidated zone is reduced, resulting in lesser relative gain in ultimate break-out capacity.

4.3 Maximum partially consolidated undrained capacity

The methodology for calculating consolidated undrained capacity discussed in the preceding sections are applicable for cases with completion of full primary consolidation. However, there may be insufficient time between installation and start of operation of the pipelines for dissipation of all the excess pore-water pressures to be feasible. In those cases, the gain in capacity will depend on the degree of partial consolidation. The maximum, partially consolidated, undrained capacities ($V_{max,PCU}$ and $H_{max,PCU}$) for different non-dimensional time periods (T = 0.05, 0.5 and 100 which is equivalent to 30%, 75% and 100% degree of consolidation) are evaluated in a similar way as described in the previous section. The development of ultimate horizontal and vertical capacities is directly associated with the extent of excess pore pressure dissipation during partial consolidation. The ratio of ultimate, partially consolidated to unconsolidated capacities are shown to vary with the preload as exhibited in Fig. 15. These variations for maximum vertical and horizontal resistances can be fitted separately as given below:

$$\frac{V_{max,PCU}}{V_{max,UU}} = 1 + a_d \left[\left(1 - \frac{\Delta u}{\Delta u_{i,p}} \right) \left(\frac{V_p}{V_{max,UU}} \right) \right]^{b_d} \tag{16}$$

$$\frac{H_{max,PCU}}{H_{max,UU}} = 1 + c_d \left[\left(1 - \frac{\Delta u}{\Delta u_{i,p}} \right) \left(\frac{V_p}{V_{max,UU}} \right) \right]^{d_d} \tag{17}$$

The term $(1-\Delta u/\Delta u_{i,p})$ in the above expressions is the measure of excess pore-water pressure dissipated during partial consolidation and is equal to 1 for full primary consolidation. The variation of $(\Delta u/\Delta u_{i,p})$ near the pipe invert is previously defined in Eq. (6). Values of the fitting parameter, m used in Eq. (6) are kept constant for different installation depths, whereas the non-dimensional time factors for 50% decay in excess pore-water pressure ($T_{50,V}$ and $T_{50,H}$) are varied to best-fit the maximum, partially consolidated vertical and horizontal resistance responses (refer to Table 7 for the values of non-dimensional time factors). The set of fitting

coefficients (a_d, b_d) for $V_{max,PCU}$ and (c_d, d_d) for $H_{max,PCU}$ are the same as used for fully consolidated, maximum undrained capacities (see Table 5).

4.4 Normalized failure envelopes

The failure envelopes presented in section 3.3 (see Figs. 8, 10 and 11) vary markedly with the preload level at a particular embedment depth. To generalise this variation, the fully consolidated vertical and horizontal capacities are normalized with their respective maximum values predicted from Eqs. (10) and (11). Fig. 16(a) shows a typical variation of normalized *V*-*H* resistances at w/D = 0.25, where all the capacities for different preloads and break-out directions fall within a tight band and thus can be expressed by an elliptical envelope of the skewed form (Martin and Houlsby, 2000):

$$\frac{H_{CU}}{H_{max,CU}} = \beta \left(\frac{V_{CU}}{V_{max,CU}} \right)^{\beta_1} \left(1 - \frac{V_{CU}}{V_{max,CU}} \right)^{\beta_2} \tag{18}$$

$$\beta = \frac{(\beta_1 + \beta_2)^{(\beta_1 + \beta_2)}}{\beta_1^{\beta_1} \beta_2^{\beta_2}} \tag{19}$$

where, β_1 and β_2 are the curve fitting parameters that controls the skewness of the envelope, and the values are listed in Table 8 for various penetration depths.

The *V*-*H* resistances for partial consolidation cases (T = 0.05 and 0.5) are also normalized with respect to their corresponding maximum capacities obtained from Eqs. (16) and (17), and the results are shown in Fig. 16(a). Since the values are very close to the normalized fully consolidated capacities, all cases can be described by the same elliptical envelope as in Eq. (18). All the analyses were repeated for other embedment levels (w/D = 0.5 and 1), and the normalized failure envelopes for all combinations of pipe weight and degree of consolidation are derived [see Fig. 16(b)].

5. Conclusions

Effects of dissipation of installation induced pore-water pressure on the lateral break-out behaviour of deep-water pipelines were investigated in this study. The installation of the pipeline was simulated by a series of LDFE analyses, and the subsequent consolidation and break-out behaviour investigated through SSFE analyses. In both the LDFE and SSFE analyses, the MCC soil constitutive model was used to capture changing undrained shear strength with installation and subsequent consolidation. The study considers a much greater range of variables than previous studies have considered, including range of pipe weights, embedment depths, and degrees of consolidation, - with installation effects incorporated to evaluate the lateral break-out resistance. Results from this comprehensive study have then been encapsulated to develop a generalized predictive model usable for design, that has not been proposed before. Moreover, the current design guideline for on-bottom pipelines (DNV GL RP-F114, 2017) does not consider the effect of shear strength enhancement due to consolidation, and unconsolidated undrained soil behaviour is assumed for the estimation of pipe break-out resistance. The paper addresses the key effect of this assumption, which is a significant novelty in research and practice.

The findings showed, as expected, that the combined capacity of the pipe, expressed in terms of *V*-*H* failure envelopes, increases with the increase in embedment depth, preload level and degree of consolidation. The effects of installation, drainage, and associated consolidation on the break-out response of on-bottom pipeline were quantified and simple equations are provided as a predictive methodology to facilitate application in design. Comparison of results between large deformation and small strain analysis demonstrates that LDFE analysis is necessary to capture the behavioural response of pipelines installed in soft clay seabed. For example, the consolidation time for 50% dissipation of excess pore-water pressure near the pipe invert is enhanced by a factor of 1.5 at $w/D = 0.5$ in LDFE analysis compared to SSFE results, due to the formation of soil berms either side of the pipe during installation. This is a

critical aspect from the pipe operational point of view as the decay in excess pore pressure response governs the timescale for the rate of gain in soil shear strength. The development of ultimate vertical and horizontal capacities is also associated with the degree of improvement in shear strength of the surrounding soil post consolidation. The mechanism of failure is influenced by the depth of soil berms developed around the pipe during installation. It is, therefore, necessary to explicitly capture the effect of the pipe penetration process for the assessment of lateral break-out resistance of seabed pipelines installed in clay including the effects of drainage and consolidation. Without considering large deformations of soil associated with the installation, consolidated break-out capacity would be underpredicted by between 10% - 50% depending on embedment ratio.

CRediT authorship contribution statement

Bithin Ghorai: Software, Validation, Formal analysis, Investigation, Writing – original draft, Visualization. **Santiram Chatterjee**: Conceptualization, Methodology, resources, Writing – review & editing, Supervision, Funding acquisition. **Susan Gourvenec**: Conceptualization, writing – review & editing.

Declaration of Competing Interest

The authors declare that they have no known competing financial interests or personal relationships that could appeared to influence the work reported in this paper.

Acknowledgement

Funding: This work was supported by the Science and Engineering Research Board, Department of Science and Technology, Government of India [grant number YSS/2014/000628/ES]. Susan Gourvenec is supported by the Royal Academy of Engineering under the Chairs in Emerging Technologies scheme.

References

[Krost et al., 2011] K. Krost, S.M. Gourvenec, D.J. White, Consolidation around partially embedded seabed pipelines, Géotechnique 61 (2) (2011) 167-173. http://dx.doi.org/10.1680/geot.8.T.015.

[Randolph and White, 2008] M.F. Randolph, D.J. White, Upper-bound yield envelopes for pipelines at shallow embedment in clay, Géotechnique 58 (4) (2008) 297-301. http://doi: 10.1680/geot.2008.58.4.297.

[Merifield et al., 2008] R.S. Merifield, D.J. White, M.F. Randolph, The ultimate undrained resistance of partially embedded pipelines, Géotechnique 58 (6) (2008) 461-470. http://doi: 10.1680/geot.2008.58.6.461.

[Wang et al., 2010] D. Wang, D.J. White, M.F. Randolph, Large-deformation finite element analysis of pipe penetration and large-amplitude lateral displacement, Can. Geotech. J. 47 (8) (2010) 842-856. http://dx.doi.org/10.1139/T09-147.

[Chatterjee et al., 2012a] S. Chatterjee, M.F. Randolph, D.J. White, The effects of penetration rate and strain softening on the vertical penetration resistance of seabed pipelines, Géotechnique 62 (7) (2012a) 573-582. http://dx.doi.org/10.1680/geot.10.P.075.

[Chatterjee et al., 2012b] S. Chatterjee, M.F. Randolph, D.J. White, Numerical simulations of pipe-soil interaction during large lateral movements on clay, Géotechnique 62 (8) (2012b) 693-705. http://doi: 10.1680/geot.10. P.107.

[Ghorai and Chatterjee, 2017] B. Ghorai, S. Chatterjee, Influences of strain rate and soil remoulding on initial break-out resistance of deepwater on-bottom pipelines, Comput. Geotech. 91 (2017) 82-92. https://doi.org/10.1016/j.compgeo.2017.07.006.

[Dingle et al., 2008] H.R.C. Dingle, D.J. White, C. Gaudin, Mechanisms of pipe embedment and lateral breakout on soft clay, Can. Geotech. J. 45 (5) (2008) 636-652. http://dx. doi.org/10.1139/T08-009.

[White and Dingle, 2011] D.J. White, H.R.C. Dingle, The mechanism of steady 'friction' between seabed pipelines and clay soils, Géotechnique 61 (12) (2011) 1035-1041. http://doi: 10.1680/geot.8. T.036.

[Rismanchian et al., 2019] A. Rismanchian, D.J. White, M.F. Randolph, C.M. Martin, Shear strength of soil berm during lateral buckling of subsea pipelines, Appl. Ocean Res. 90 (2019) 101864. https://doi.org/10.1016/j/apor.2019.101864.

[Gourvenec and White, 2010] S. Gourvenec, D. White, Elastic solutions for consolidation around seabed pipelines, in: Proceedings of Offshore Technology Conference, Houston, USA, 2010, OTC 20554. http://dx.doi.org/10.4043/20554-MS.

[Chatterjee et al., 2012c] S. Chatterjee, Y. Yan, M.F. Randolph, D.J. White, Elastoplastic consolidation beneath shallowly embedded offshore pipelines, Géotech. Lett. 2 (2) (2012c) 73-79. http://dx.doi.org/10.1680/geolett.12.00031.

[Chatterjee et al., 2013] S. Chatterjee, D.J. White, M.F. Randolph, Coupled consolidation analysis of pipe–soil interactions, Can. Geotech.

J. 50 (6) (2013) 609-619. http://dx.doi.org/10.1139/cgj-2012-0307.

[Chatterjee et al., 2014] S. Chatterjee, S. Gourvenec, D.J. White, Assessment of the consolidated breakout response of partially embedded subsea pipelines, Géotechnique 64 (5) (2014) 391-399. http://dx.doi.org/10.1680/geot.13.P.215.

[Cocjin et al., 2018] M.L. Cocjin, S.M. Gourvenec, D.J. White, Softening and consolidation around seabed pipelines: centrifuge modelling, Géotechnique 68 (2) (2018) 118-132. https://doi.org/10.1680/jgeot.16.P.280.

[Westgate et al., 2009] Z.J. Westgate, D.J. White, M.F. Randolph, Video observations of dynamic embedment during pipelaying in soft clay, in: Proceedings of the ASME 28th International Conference on Ocean, Offshore and Arctic Engineering OMAE2009, Honolulu, Hawaii, USA, 2009, OMAE2009-79814. https://doi.org/10.1115/OMAE2009-79814.

[Hu and Randolph, 1998a] Y. Hu, M.F. Randolph, A practical numerical approach for large deformation problems in soil, Int. J. Numer. Anal. Methods Geomech. 22 (5) (1998a) 327-350. http://dx.doi.org/10.1002/(SICI)1096-9853(199805) 22:5%3C327::AID-NAG920%3E3.0.CO;2-X.

[Hu and Randolph, 1998b] Y. Hu, M.F. Randolph, H-adaptive FE analysis of elasto-plastic non-homogeneous soil with large deformation, Comput. Geotech. 23 (1-2) (1998b) 61-83. http://dx.doi.org/10.1016/S0266-352X (98)00012-3.

[Roscoe and Burlund, 1968] K.H. Roscoe, J.B. Burland, On the generalised stress–strain behaviour of 'wet clay', in: Engineering plasticity, 535–609, Cambridge, UK: Cambridge University Press, 1968.

[Dassault Systèmes, 2013] Dassault Systèmes, ABAQUS 6.13 analysis user's guide, Providence, RI, USA: Simulia Corp, (2013).

[Merifield et al., 2009] R.S. Merifield, D.J. White, M.F. Randolph, Effect of surface heave on response of partially embedded pipelines on clay, J. Geotech. Geoenviron. Eng. 135 (6) (2009) 819-829. http://dx.doi.org/10.1061/(ASCE)GT.1943-5606.0000070.

[Martin and White, 2012] C.M. Martin, D.J. White, Limit analysis of the undrained bearing capacity of offshore pipelines, Géotechnique 62 (9) (2012) 847-863.

[Dutta et al., 2015] S. Dutta, B. Hawlader, R. Phillips, Finite element modeling of partially embedded pipelines in clay seabed using Coupled Eulerian-Lagrangian method, Can. Geotech. J. 52 (1) (2015) 58-72.

[Stewart, 1992] D.P. Stewart, Lateral loading of piled bridge abutments due to embankment construction, Ph.D. thesis, The University of Western Australia, Perth, Australia, 1992.

[Wroth, 1984] C.P. Wroth, The interpretation of in situ soil tests, Géotechnique, 34 (4) (1984) 449-489. http://dx.doi.org/10.1680/geot.1984.34.4.449.

[Ansari et al., 2014] Y. Ansari, G.P. Kouretzis, D. Sheng, An effective stress analysis of partially embedded offshore pipelines: Vertical penetration and axial walking, Comput. Geotech. 58 (2014) 69-80.

[Mahmoodzadeh et al., 2014] H. Mahmoodzadeh, M.F. Randolph, D. Wang, Numerical simulation of piezocone dissipation test in clays, Géotechnique 64 (8) (2014) 657-666.

[Mahmoodzadeh et al., 2015] H. Mahmoodzadeh, D. Wang, M.F. Randolph, Interpretation of piezoball dissipation testing in clay, Géotechnique 65 (10) (2015) 831-842. http://dx.doi.org/10.1680/jgeot.14.P.213.

[Schneider et al., 2019] M.A. Schneider, S.A. Stanier, S. Chatterjee, D.J. White, M.F. Randolph, The parkable piezoprobe for determining c_v and strength-modelling and interpretation methods, Géotechnique 69 (5) (2019) 458-469. http://dx.doi.org/10.1680/jgeot.18.P.004.

[Hodder and Cassidy, 2010] M.S. Hodder, M.J. Cassidy, A plasticity model for predicting the vertical and lateral behaviour of pipelines in clay soils, Géotechnique 60 (4) (2010) 1035-1041. http://doi.org/10.1680/geot.8. P.055.

[Gourvenec et al., 2014] S.M. Gourvenec, C. Vulpe, T.G. Murthy, A method for predicting the consolidated undrained bearing capacity of shallow foundations, Géotechnique 64 (3) (2014) 215–225. http://dx.doi.org//10.1680/geot.13.P.101.

[Feng and Gourvenec, 2015] X. Feng, S. Gourvenec, Consolidated undrained load-carrying capacity of subsea mudmats under combined loading in six degrees of freedom, Géotechnique 65 (7) (2015) 563–575. http://dx.doi.org//10.1680/geot.14.P.090.

[Stanier and White, 2019] S.A. Stanier, D.J. White, Enhancement of bearing capacity from consolidation: due to changing strength or failure mechanism, Géotechnique, 69 (2) (2019) 166–173. http://dx.doi.org//10.1680/geot.17.T.03.

[Martin and Houlsby, 2000] C.M. Martin, G.T. Houlsby, Combined loading of spudcan foundations on clay: laboratory tests, Géotechnique 50 (4) (2000) 325-338. https://doi.org/10.1680/geot.2000.50.4.325.

[DNV GL RP-F114, 2017] DNV GL RP-F114, Pipe soil interaction for submarine pipelines, Det Norske Veritas AS, Høvik, Norway, Edition May 2017, (2017).

List of Tables

Table 1
Pipe-soil parameters used in coupled LDFE analysis.

Parameters	Values
Pipe diameter (D)	0.5 m
Slope of CSL in p'-q space (M) or	0.92
internal friction angle in triaxial compression (φ'_{cs})	23.5°
Void ratio on CSL (e_{cs}) at p' = 1kPa	2.14
Slope of NCL in e-ln(p') space (λ)	0.205
Slope of URL in e-ln(p') space (κ)	0.044
Wet yield surface size parameter (β_{yield})	1.0
Flow stress ratio (K)	1.0
Permeability of soil (k)	1×10^{-9} m/s
Unit weight of water (γ_w)	10 kN/m^3
Uniform surcharge at seabed level (σ'_{v0})	10 kPa
Drained Poisson's ratio (v')	0.3
Pipe-soil interface	Smooth
Incremental displacement in LDFE analysis (δ)	1% of D

Table 2
Various analyses cases considered in the study.

Parameters	Values
Pipe embedment level (w/D)	0.25, 0.5, 1
Normalized preload ($V_p/V_{max,UU}$)	0.3, 0.6, 0.75, 0.9
Non-dimensional consolidation time ($T = c_v t/D^2$)	0.05, 0.5, 100
(degree of consolidation)	(30%, 75%, 100%)
Breakout directions (θ)	0°, 30°, 60°, 90°, 120°,
(with respect to upward vertical)	150°, 180°

Table 3
Normalized excess pore pressure dissipation parameters at different installation depths.

Installation depth (w/D)	T_{50}	m
0.25	0.075	1.15
0.50	0.100	1.00
1.00	0.180	0.95

Table 4
Fitting coefficients for maximum unconsolidated undrained capacities.

Unconsolidated undrained capacity	Coefficients	Values
Vertical resistance ($V_{max,UU}$)	a_u	5.73
	b_u	0.26
Horizontal resistance ($H_{max,UU}$)	c_u	2.76
	d_u	0.56

Table 5
Fitting coefficients for maximum consolidated undrained capacities.

Consolidated undrained capacity	Coefficients	Values at different pipe depths		
		w/D = 0.25	w/D = 0.5	w/D = 1
Vertical resistance ($V_{max,CU}$)	a_d	0.60	0.63	0.53
	b_d	1.20	1.40	1.20
Horizontal resistance ($H_{max,\ CU}$)	c_d	0.70	0.63	0.53
	d_d	1.40	1.40	1.40

Table 6
Combined scaling parameter for ultimate gain in consolidated vertical and horizontal capacities at various depths**.**

Consolidated undrained capacity	Values of $f_\sigma f_{su}$ at different depths		
	w/D = 0.25	w/D = 0.5	w/D = 1
Vertical resistance ($V_{max,CU}$)	0.45	0.45	0.32
Horizontal resistance ($H_{max,CU}$)	0.50	0.42	0.30

Table 7
Non-dimensional time factors for maximum partially consolidated undrained capacities at various depths.

Pipe embedment level (w/D)	$T_{50,V}$ values for vertical resistance ($V_{max,PCU}$)	$T_{50,H}$ values for horizontal resistance ($H_{max,PCU}$)	Values of m
0.25	0.08	0.06	1.15
0.50	0.09	0.08	1.00
1.00	0.25	0.18	0.95

Table 8
Fitting parameters for normalized failure envelopes at different embedments.

Pipe installation depth (w/D)	β_1	β_2
0.25	0.50	0.50
0.50	0.35	0.50
1.00	0.24	0.45

Illustration Captions

Fig. 1. Schematic of pipe-soil consolidation problem with initial mesh configuration.
Fig. 2. Comparison of vertical penetration resistances obtained from coupled LDFE analysis with theoretical and experimental solutions.
Fig. 3. Comparison of break-out responses obtained from present study with theoretical and experimental solutions.
Fig. 4. Variation of installation resistance with penetration depth (w/D = 1).
Fig. 5. Excess pore-water pressure field around the pipe after installation: (a) w/D = 0.25, (b) w/D = 0.5, (c) w/D = 1.
Fig. 6. Normalized excess pore pressure dissipation time history near pipe invert: (a) normalized with initial value under respective preloads during consolidation, (b) at different installation depths [Eq. (6)].
Fig. 7. Consolidation settlement of pipe under different preloads at w/D = 0.25.
Fig. 8. Fully consolidated undrained failure envelopes under different preload levels at: (a) w/D = 0.25, (b) w/D = 0.5, and (c) w/D = 1.
Fig. 9. Contours of shear strength enhancement after consolidation under different preloads at w/D = 0.25: (a) $V_p/V_{max,UU}$ = 0.3, (b) $V_p/V_{max,UU}$ = 0.6, (c) $V_p/V_{max,UU}$ = 0.75, (d) $V_p/V_{max,UU}$ = 0.9.
Fig. 10. Partially consolidated undrained failure envelopes under various preloads for T = 0.05 (30% degree of consolidation) at: (a) w/D = 0.25, (b) w/D = 0.5, and (c) w/D = 1.
Fig. 11. Partially consolidated undrained failure envelopes under various preloads for T = 0.5 (75% degree of consolidation) at: (a) w/D = 0.25, (b) w/D = 0.5, and (c) w/D = 1.
Fig. 12. Maximum unconsolidated undrained vertical and horizontal capacities.
Fig. 13. Maximum consolidated undrained capacities at different installation depths: (a) vertical resistance, and (b) horizontal resistance.
Fig. 14. Development of fully consolidated undrained capacity under various preloads due to gain in soil shear strength: (a) maximum vertical resistance, and (b) maximum horizontal resistance.
Fig. 15. Maximum partially consolidated undrained capacities for various consolidation time periods (w/D = 0.25): (a) vertical resistance, and (b) horizontal resistance.
Fig. 16. Consolidated undrained failure envelopes: (a) normalized by maximum capacities at w/D = 0.25, (b) at various installation depths.

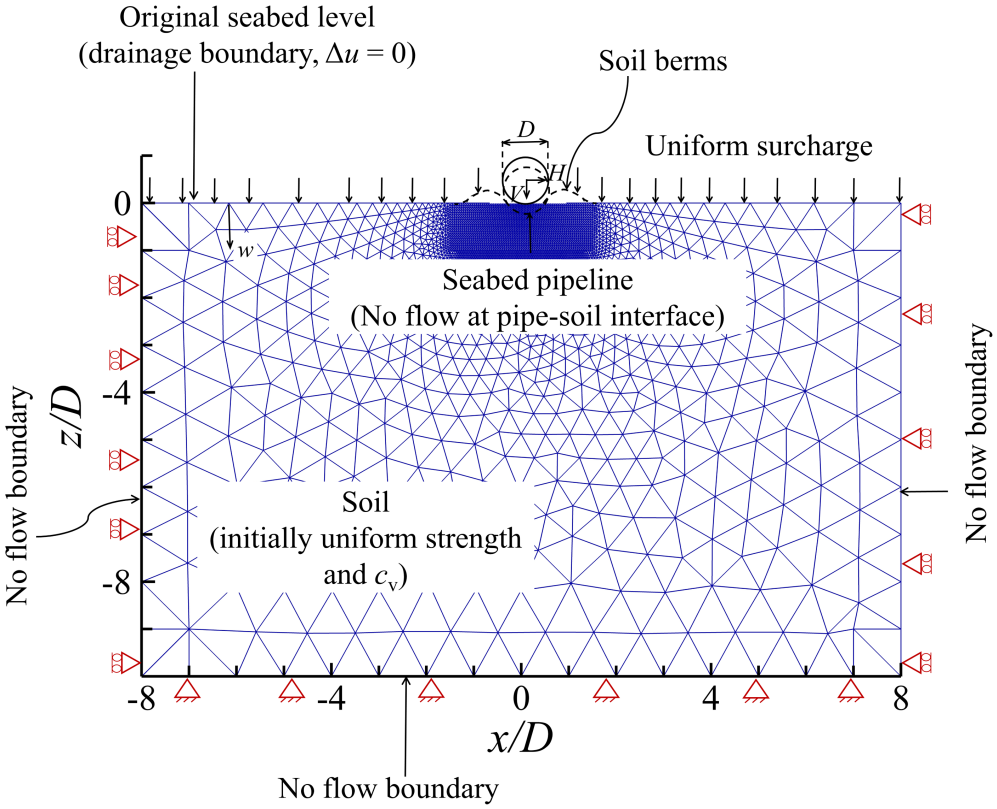

Fig. 1. Schematic of pipe-soil consolidation problem with initial mesh configuration.

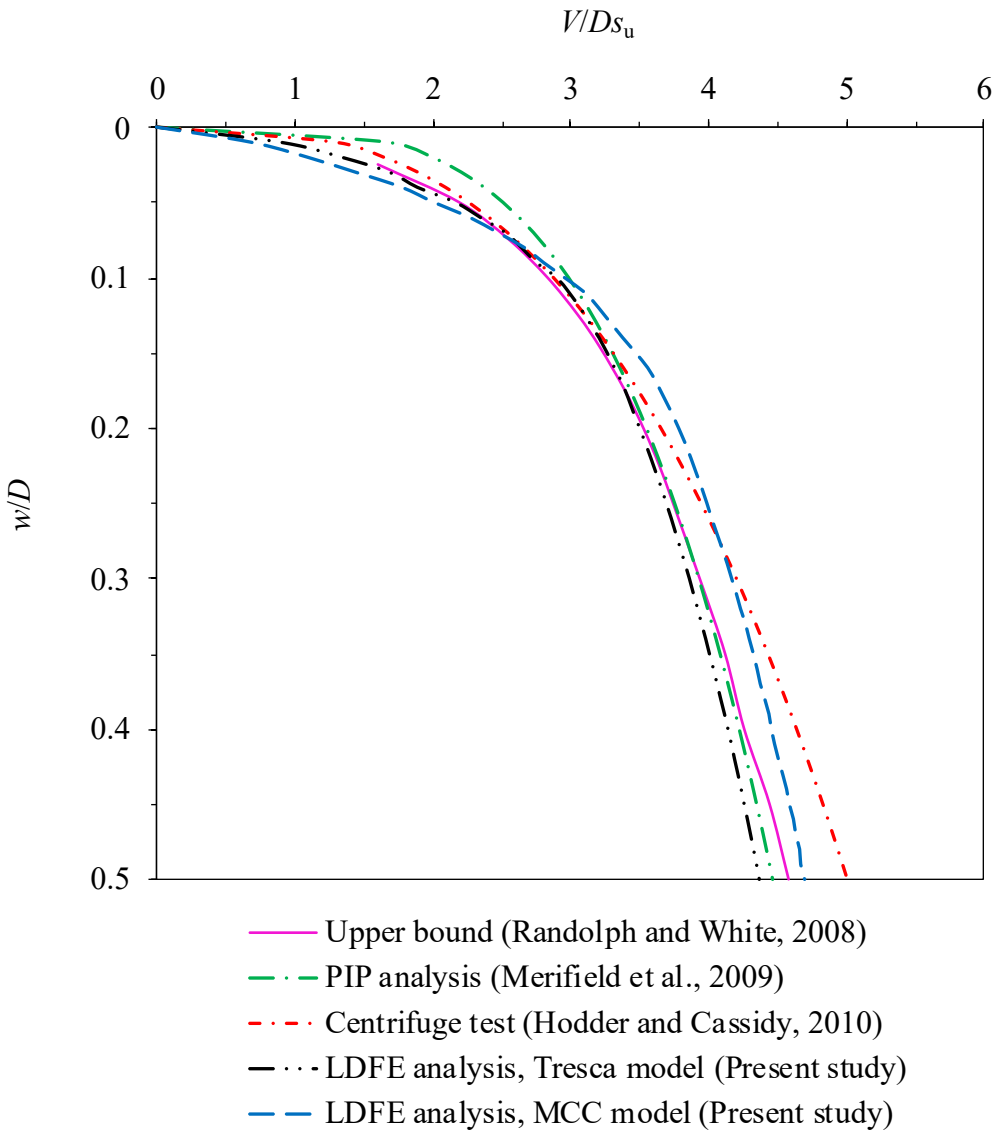

Fig. 2. Comparison of vertical penetration resistances obtained from coupled LDFE analysis with theoretical and experimental solutions.

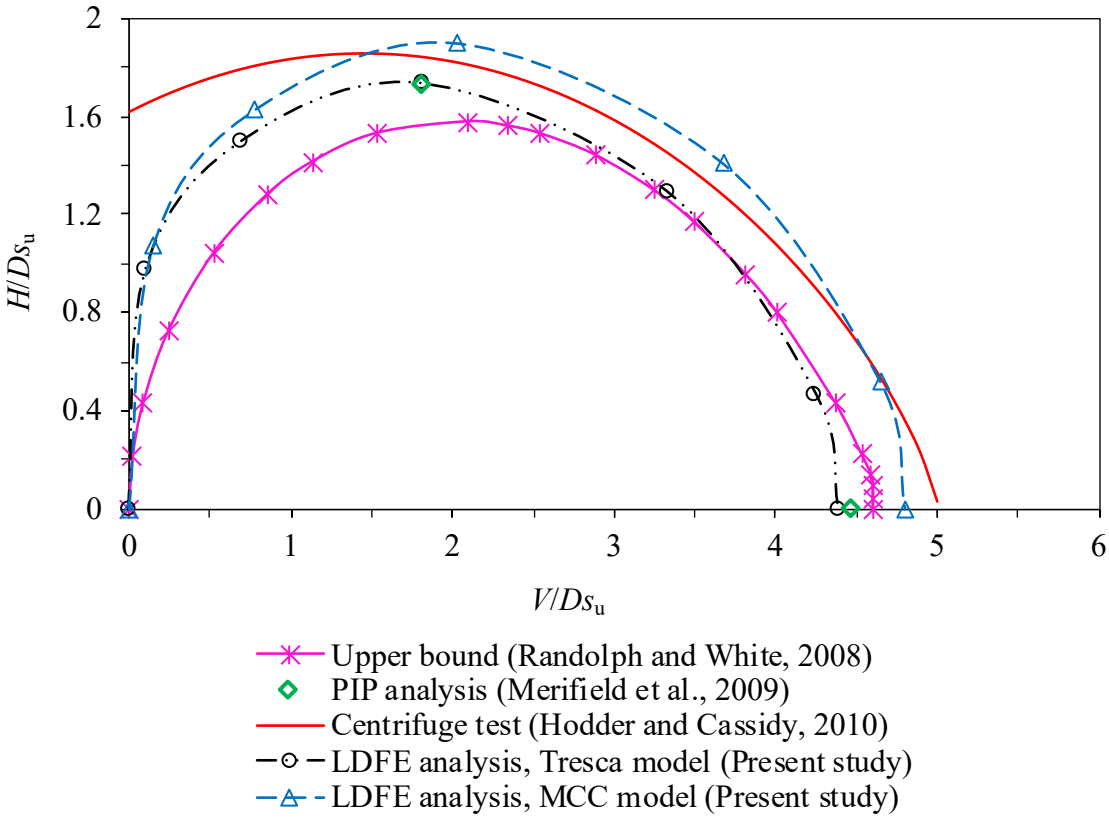

Fig. 3. Comparison of break-out responses obtained from present study with theoretical and experimental solutions.

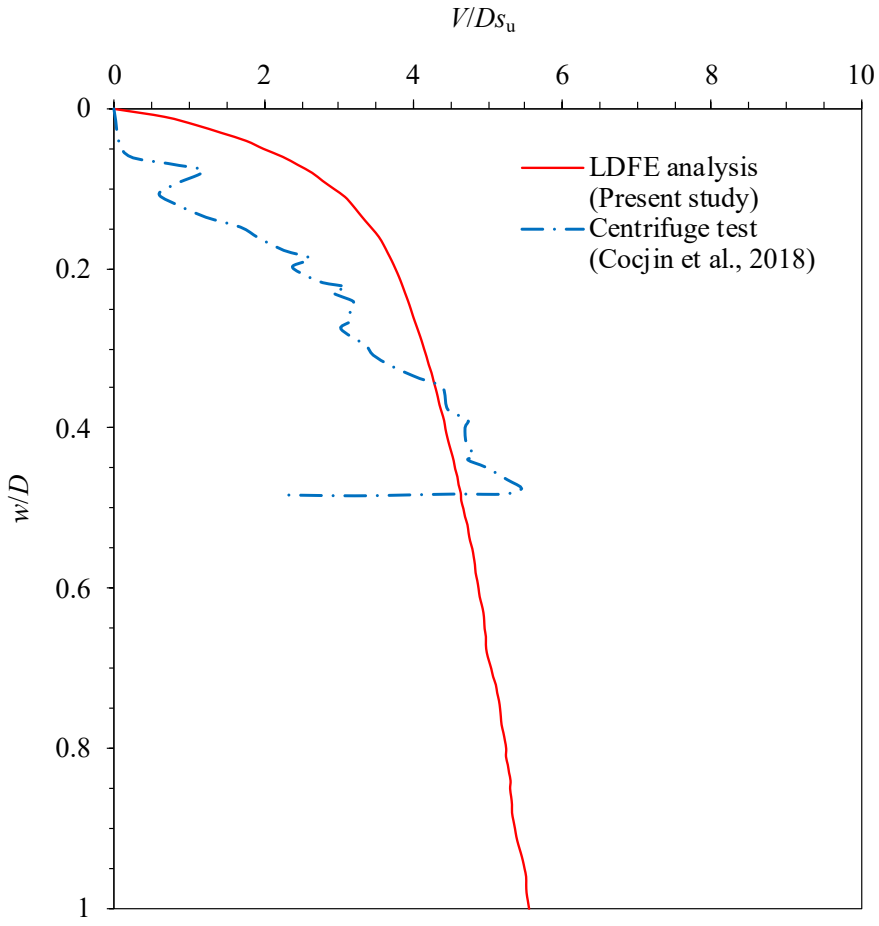

Fig. 4. Variation of installation resistance with penetration depth (w/D = 1).

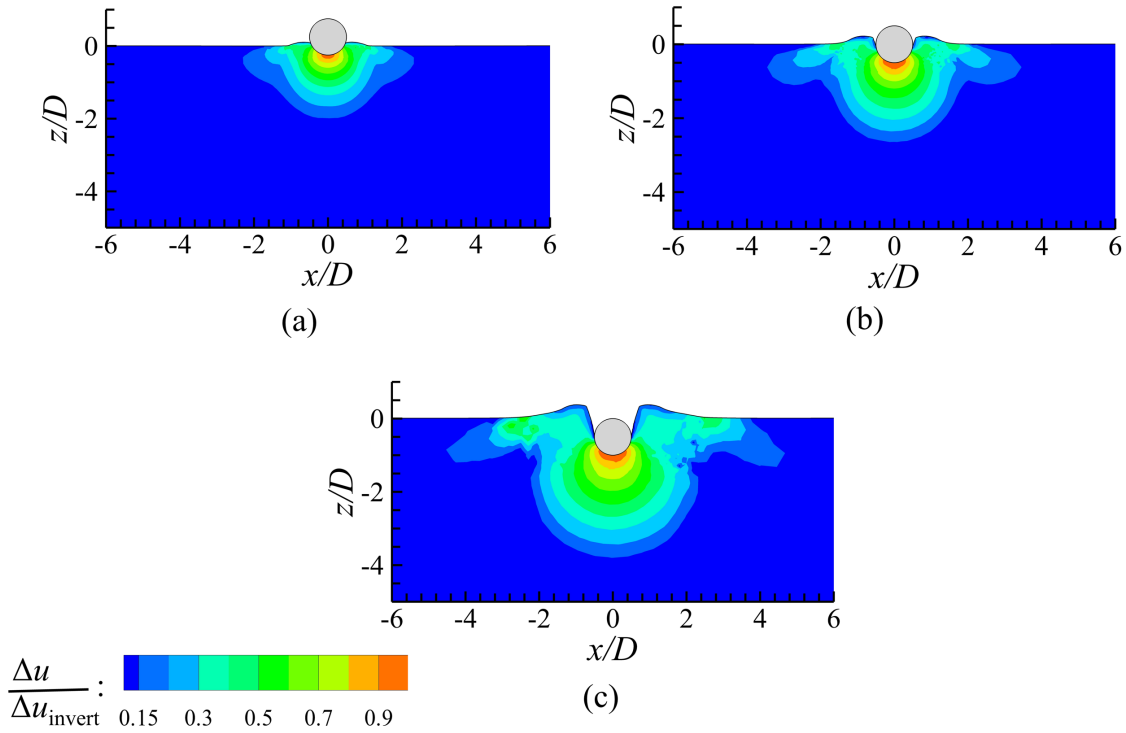

Fig. 5. Excess pore-water pressure field around the pipe after installation: (a) $w/D = 0.25$, (b) $w/D = 0.5$, (c) $w/D = 1$.

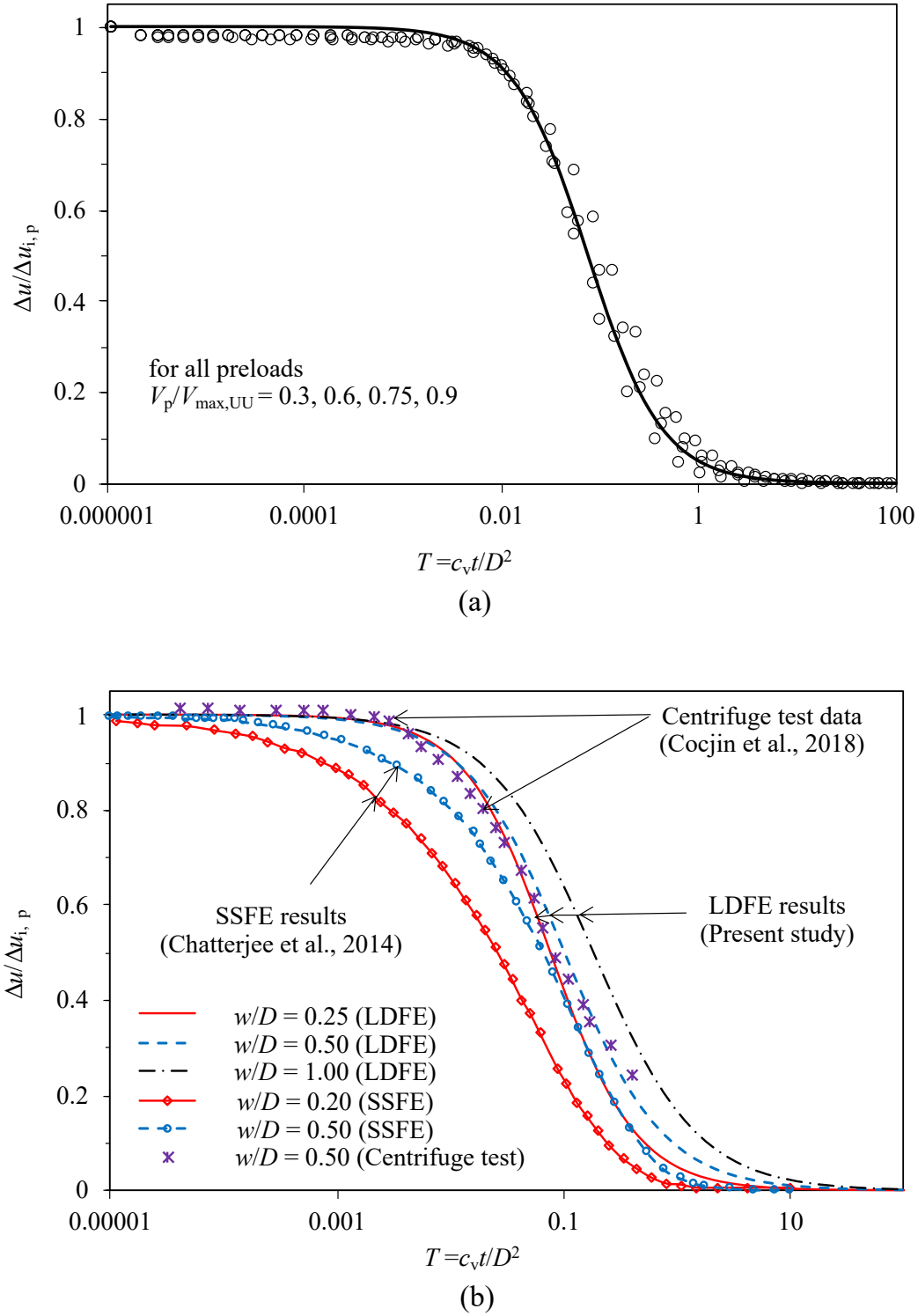

Fig. 6. Normalized excess pore pressure dissipation time history near pipe invert: (a) normalized with initial value under respective preloads during consolidation, (b) at different installation depths [Eq. (6)].

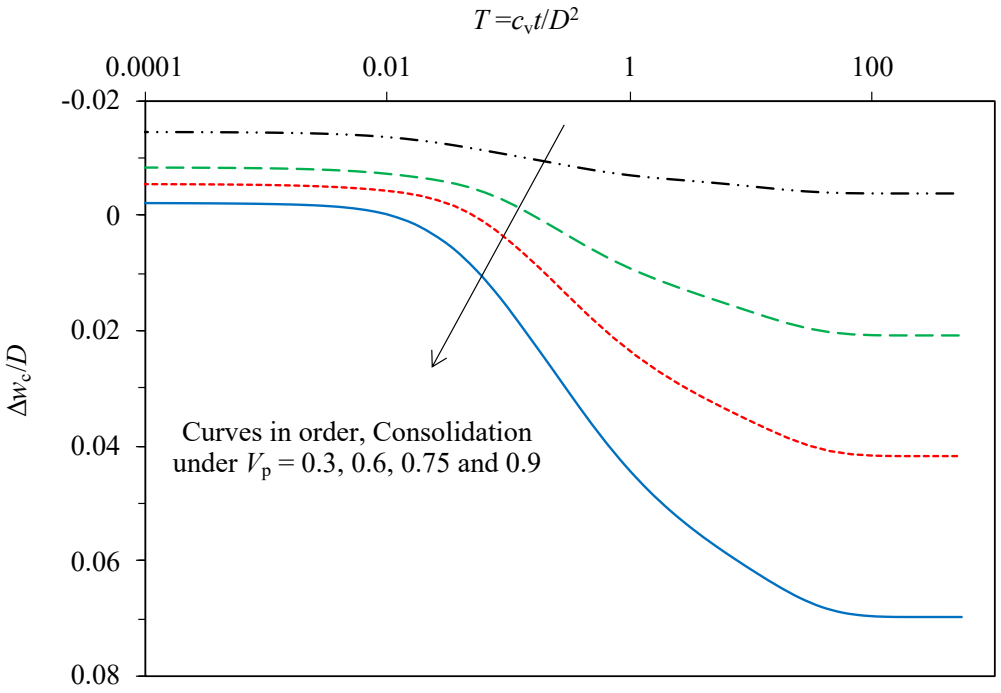

Fig. 7. Consolidation settlement of pipe under different preloads at $w/D = 0.25$.

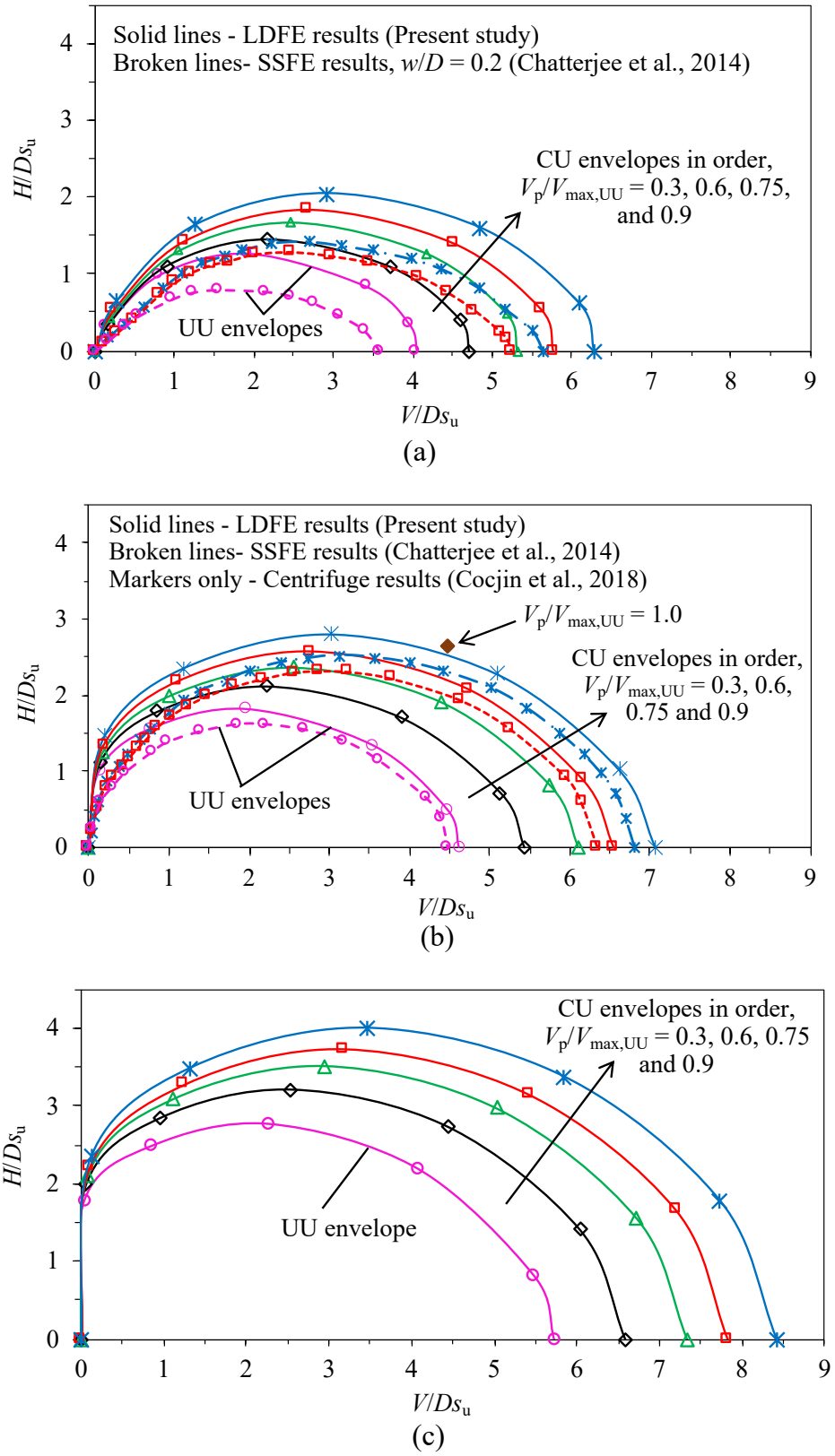

Fig. 8. Fully consolidated undrained failure envelopes under different preload levels at: (a) $w/D = 0.25$, (b) $w/D = 0.5$, and (c) $w/D = 1$.

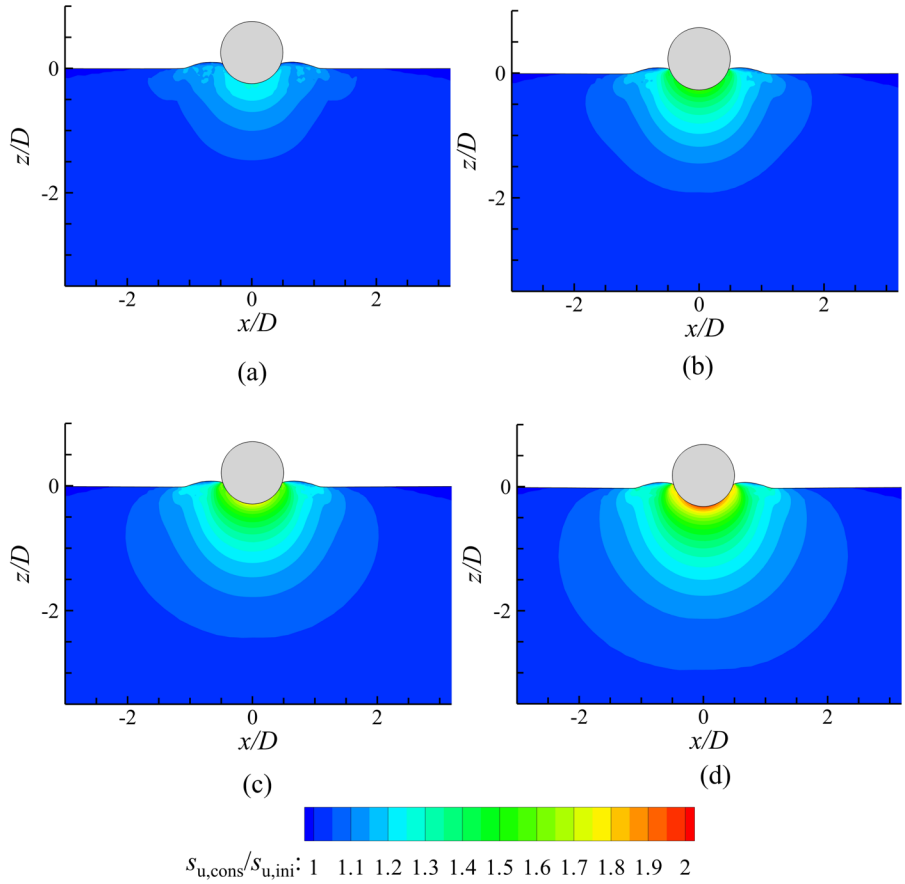

Fig. 9. Contours of shear strength enhancement after consolidation under different preloads at w/D = 0.25: (a) $V_p/V_{max,UU}$ = 0.3, (b) $V_p/V_{max,UU}$ = 0.6, (c) $V_p/V_{max,UU}$ = 0.75, (d) $V_p/V_{max,UU}$ = 0.9.

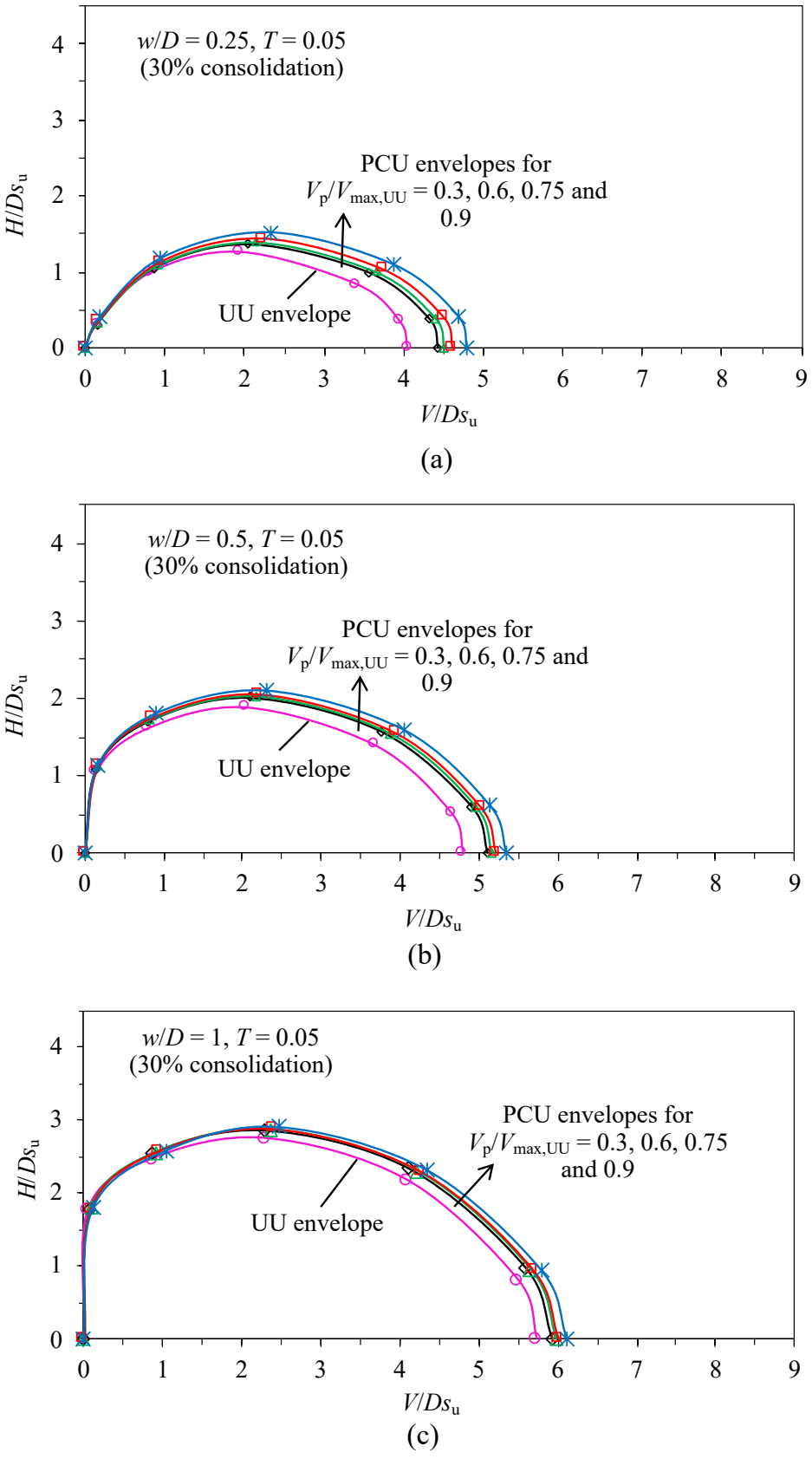

Fig. 10. Partially consolidated undrained failure envelopes under various preloads for T = 0.05 (30% degree of consolidation) at: (a) w/D = 0.25, (b) w/D = 0.5, and (c) w/D = 1.

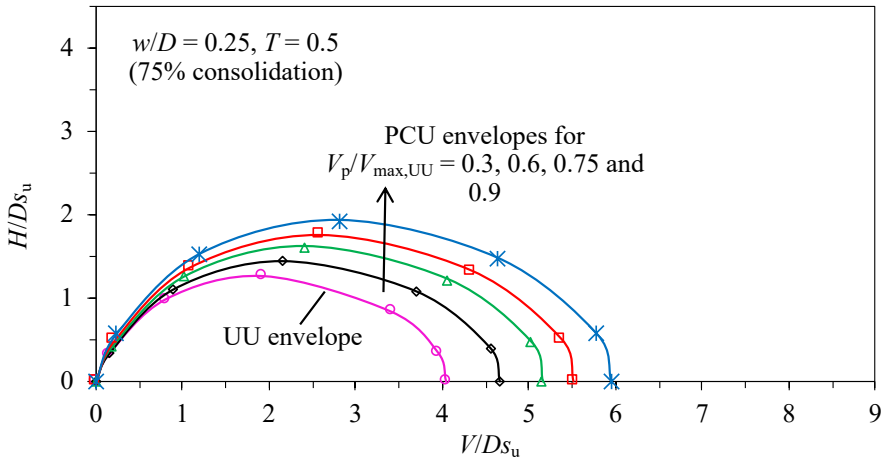

(a)

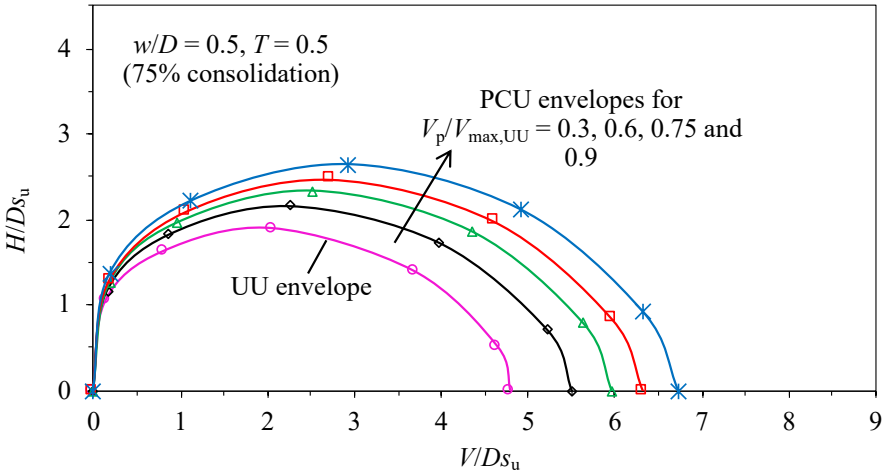

(b)

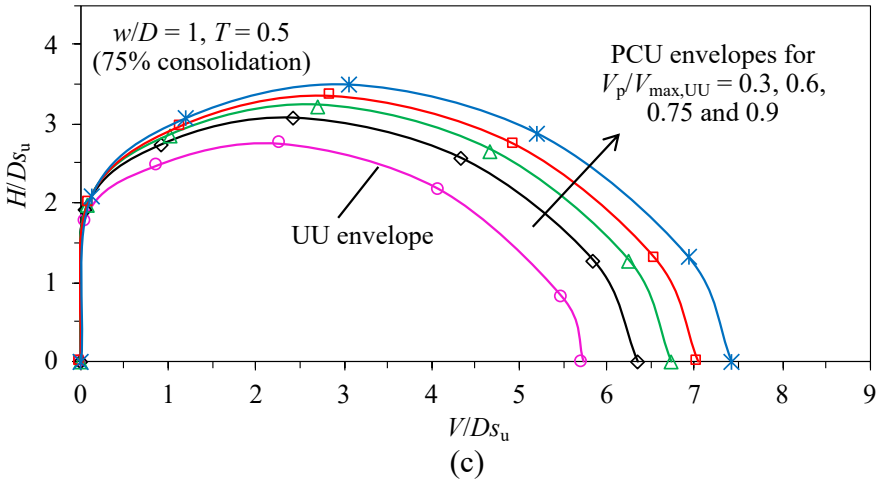

(c)

Fig. 11. Partially consolidated undrained failure envelopes under various preloads for $T = 0.5$ (75% degree of consolidation) at: (a) $w/D = 0.25$, (b) $w/D = 0.5$, and (c) $w/D = 1$.

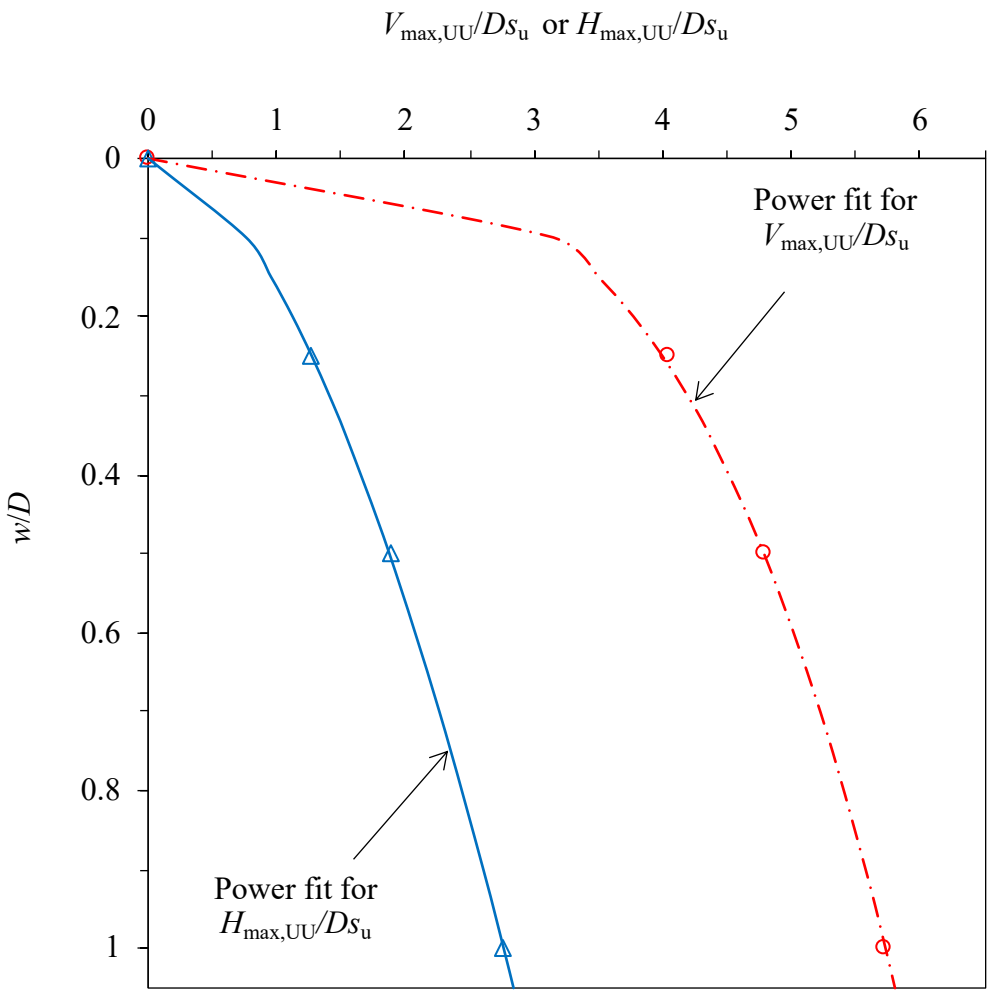

Fig. 12. Maximum unconsolidated undrained vertical and horizontal capacities.

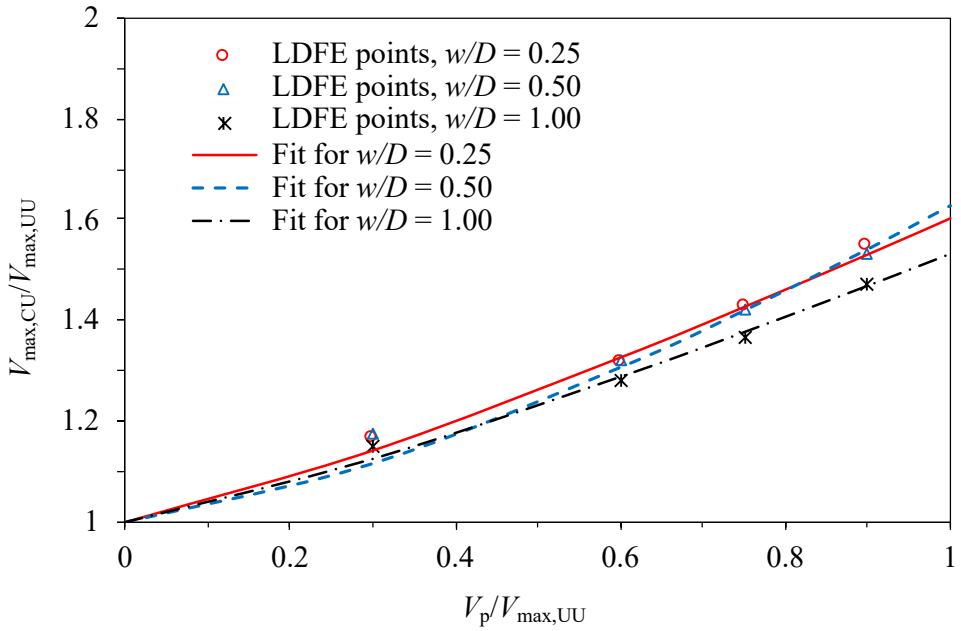

(a)

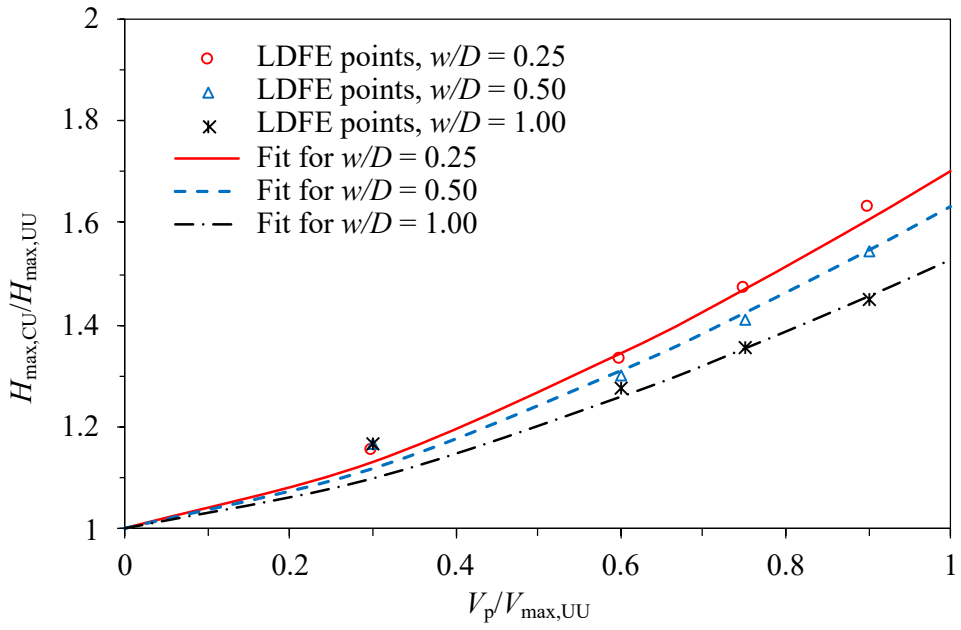

(b)

Fig. 13. Maximum consolidated undrained capacities at different installation depths: (a) vertical resistance, and (b) horizontal resistance.

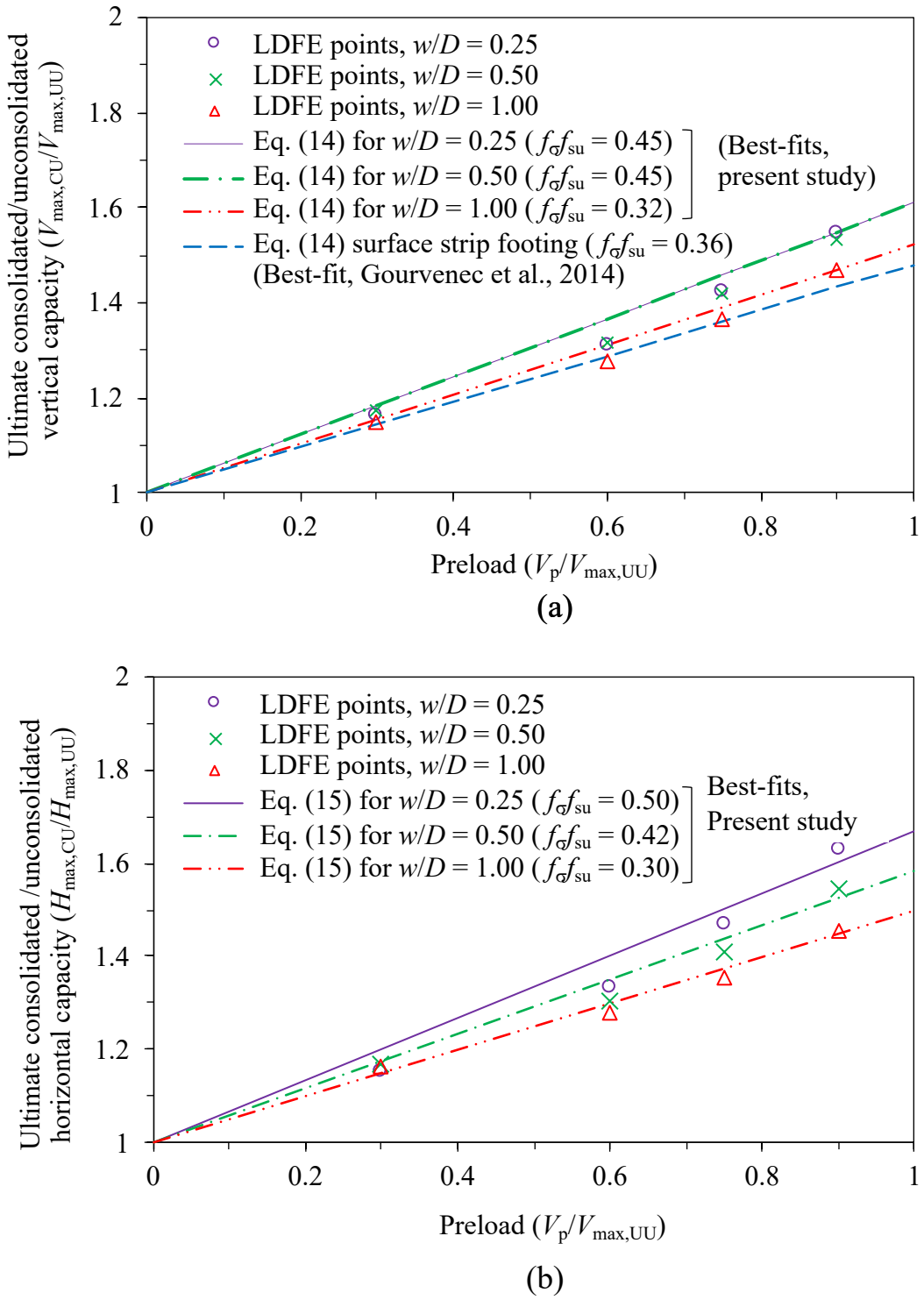

Fig. 14. Development of fully consolidated undrained capacity under various preloads due to gain in soil shear strength: (a) maximum vertical resistance, and (b) maximum horizontal resistance.

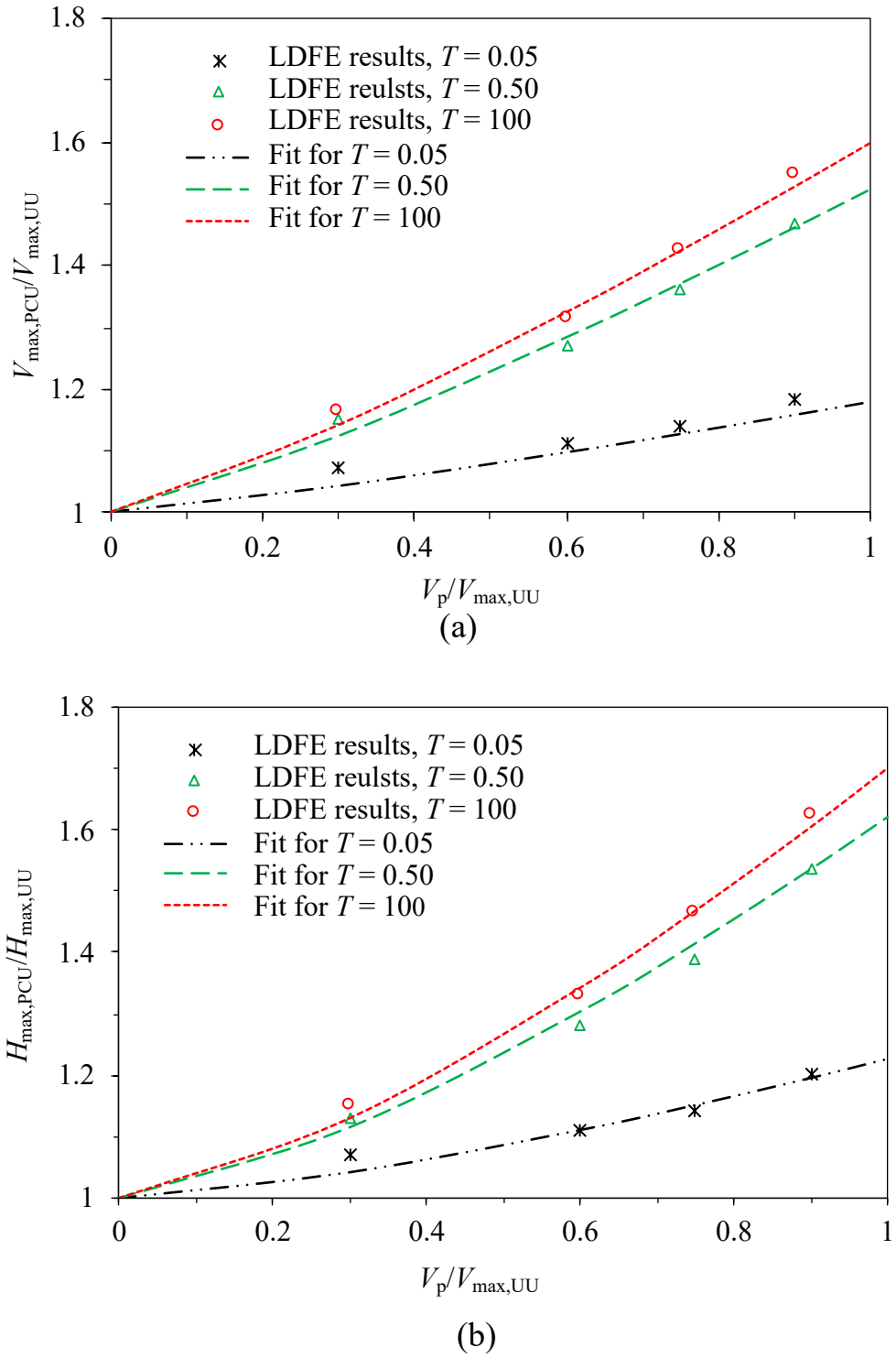

Fig. 15. Maximum partially consolidated undrained capacities for various consolidation time periods (w/D = 0.25): (a) vertical resistance, and (b) horizontal resistance.

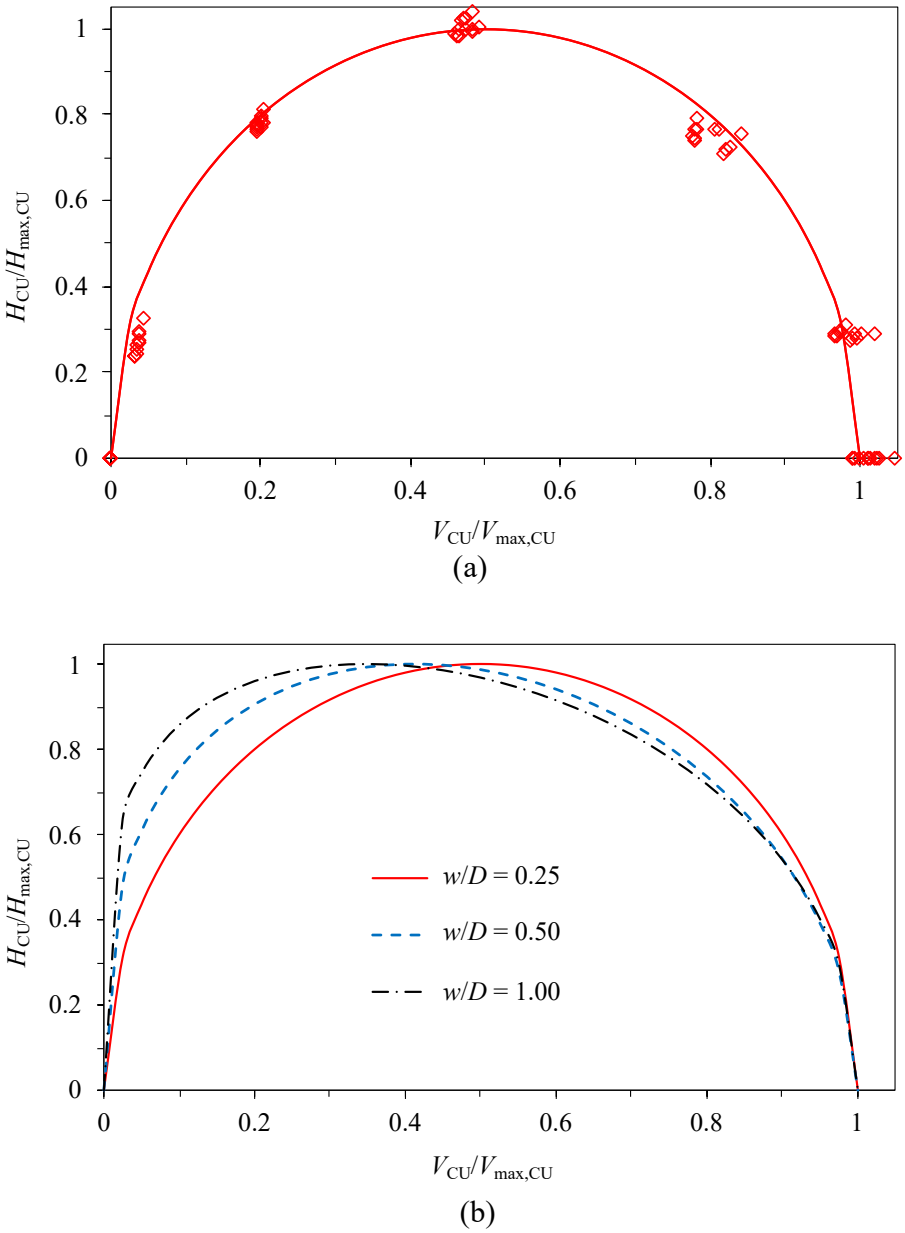

Fig. 16. Consolidated undrained failure envelopes: (a) normalized by maximum capacities at w/D = 0.25, (b) at various installation depths.